Targeting adequate thermal stability and fire safety in selecting ionic liquid-based electrolytes for energy storage

Léa Chancelier, Alpha-Oumar Diallo, Catherine Santini, Guy Marlair, Thibaut Gutel, Sophie Mailley, Christophe Len

Targeting adequate thermal stability and fire safety in selecting ionic liquid-based electrolytes for energy storage †

L. Chancelier,[a,b] A.O. Diallo,[c,d] C.C. Santini,*[a] G. Marlair,*[c] T. Gutel,[b] S. Mailley,[b] C. Len[d]

(a) UMR 5265 CNRS-Université de Lyon 1-ESCPE Lyon, 43 Boulevard du 11 Novembre 1918, 69616 Villeurbanne, France

(b) CEA, LITEN (LMB), 17 rue des martyrs, 38054 Grenoble, France

(c) Institut National de l'Environnement Industriel et des Risques (INERIS), Parc Technologique Alata, BP2, 60550 Verneuil-en-Halatte, France

(d) UTC–ESCOM, EA 4297, TIMR, Centre de Recherches de Royallieu, BP 20529, 60205 Compiègne, France

† Electronic Supplementary Information (ESI) available

Corresponding author: catherine.santini@univ-lyon1.fr

Abstract

The energy storage market relating to lithium based systems regularly grows in size and expands in terms of portfolio of energy and power demanding applications. Thus safety focused research must more than ever accompany related technological breakthroughs regarding performance of cells, resulting in intensive research on the chemistry and material science to design more reliable battery. Formulating electrolyte solutions with nonvolatile and nonflammable ionic liquids instead of actual carbonate mixtures could be safer. However, few definitions of thermal stability of electrolytes based on ionic liquids have been reported in case of abuse conditions (fire, shortcut, overcharge or overdischarge). This work investigates thermal stability up to combustion of 1-butyl-3-methylimidazolium bis(trifluoromethanesulfonyl)imide ($[C_1C_4Im][NTf_2]$) and 1-butyl-1-methylpyrrolidinium bis(trifluoromethanesulfonyl)imide ($[PYR_{14}][NTf_2]$) ionic liquids, and their corresponding electrolytes containing lithium bis(trifluoromethanesulfonyl)imide $[Li][NTf_2]$. Their possible routes of degradation during thermal abuse testings were investigated by thermodynamic studies under several experimental conditions. Their behaviours under fire were also tested, including the analysis of emitted compounds.

Keywords: Ionic liquids, electrolytes, thermal stability, combustion behaviour

1. Introduction

Environmental concerns and security of energy supply are key drivers for the promotion of a new generation of energy storage systems. These systems must be capable of addressing a number of technical challenges for the sustainable development of electromobility (terrestrial, maritime and aerial to some extent). They should efficiently store intermittent renewable sources of energy (wind, sun, sea) and be part of smart grids applications.[1] Electrochemical energy storage previously had to rely on lead-acid, nickel cadmium and nickel metal hydride technologies. Commercialized since the 90s for the consumer market, lithium-ion technology and its variants have taken the lead regarding those emerging applications as they offer significantly higher power and energy densities in practice. However safety has been identified in a number of studies as a potential market restraint.[2-4]

The electrolytes of lithium-ion batteries are typically a mixture of organic carbonates like ethylene carbonate or diethylcarbonate, using lithium salt such as lithium hexafluorophosphate ($LiPF_6$) (Scheme 1). Some of the advantages of these electrolytes are their high solubility of lithium salt, good cycling efficiency, good ionic conductivity and compatibility with numerous electrode materials. Unfortunately they can lead to safety issues as they are flammable,[5] possess low flash points[6] and are not stable at high temperatures (> 60 °C).[7]

The replacement of these electrolytes by room temperature ionic liquids (ILs) is now widely considered in literature[8-12] and in industrial projects.[13-17] Indeed ILs present the required properties, such as good ionic conductivity, wide electrochemical window (4 to 6 V) and good cycling efficiency in spite of their viscosity.[18] Furthermore ILs can be safe electrolytes[19-23] as they have very low vapour pressure and high flash point.[24, 25] They are also non-flammable according to the criteria of the Globally Harmonized System,[26] and they are considered stable up to 300 °C.[27]

However thermal stability can be defined or interpreted differently, depending on the context of use. Currently, there is no standard to define the maximum operating temperature (T_{op}), even if a few attempts should be mentioned.[28, 29] When the thermal instability leads to identified dangerous properties in hazardous materials regulations, they reflect the related level of instability of the concerned materials. It can be the case for self-reactive materials,

water-reactive materials, flammable liquids, explosives… In all other cases, thermal stability keeps somewhat subjective and practical rules must be used according to intended use and desired overall performance of the system.

Contrarily to the current carbonate-based organic electrolytes,[30] few definitions of thermal stability of ILs for use as electrolytes were reported in case of abuse conditions (fire, shortcut, overcharge or overdischarge).[31] In the vast domain of ILs, imidazolium and pyrrolidinium cations associated to NTf_2 anion were selected as they showed the highest decomposition temperatures.[27, 32-36] This work investigates thermal stability up to combustion of these ILs and their corresponding electrolytes (defined as solution of ILs with 1 $mol.L^{-1}$ of lithium salt) for lithium-ion batteries. The possible routes of degradation of ILs and corresponding electrolytes during thermally abuse tests were investigated by thermodynamic studies under different experimental conditions.

2. Materials and methods

2.1. Synthesis and characterisation of the electrolytes

The ionic liquids 1-butyl-3-methylimidazoliumbis(trifluoromethanesulfonyl)imide ($[C_1C_4Im][NTf_2]$) and 1-butyl-1-methylpyrrolidiniumbis(trifluoromethanesulfonyl)imide ($[PYR_{14}][NTf_2]$) were synthesised as already reported in the literature.[37-39] (See details in SI-1 and NMR analyses in SI-2). After drying under vacuum (10^{-5} mbar) for 24 h at room temperature, the water content was lower than 60 ppm (mass ratio), as assessed by Karl Fisher coulometric titration. The absence of residual chloride (<0.5 %) was assessed by high resolution mass spectroscopy (HRMS) after several washings with water, followed by $AgNO_3$ tests.[40]

The electrolytes were prepared by adding $LiNTf_2$ (1 $mol.L^{-1}$) in a well stirred IL at room temperature, and will be referred to as $[C_1C_4Im][Li][NTf_2]$ and $[PYR_{14}][Li][NTf_2]$. Finally the neat ILs and electrolytes were vacuum-dried at room temperature for 48 h under 10^{-5} mbars followed by storage in an argon-filled glove box.

^1H, ^{13}C, ^{19}F and ^7Li solution NMR spectra were recorded at room temperature on BRUKER AVANCE 300 MHz Spectrometer with a probe 5 mm BBO with gradient of shims Z. The resonance frequencies were 300.13 MHz for ^1H, 75.48 MHz for ^{13}C, 282.38 MHz for ^{19}F and 116.64 MHz for ^7Li. Deuterated dichloromethane was used as solvent. The high resolution mass spectra (HRMS) were recorded in positive and negative ion modes on a hybrid

quadrupole time-of-flight mass spectrometer (MicroTOFQ-II, Bruker Daltonics, Bremen) with an electrospray ionization (ESI) ion source. The gas flow of the spray gas was 0.6 bar and the capillary voltage was ±4.5 kV. The solutions were infused at 180 µL.h^{-1}. The mass range of the analysis was 50 - 1000 m/z and the calibration was done with sodium formate.

2.2. Thermal stability of ILs and their electrolytes

Differential scanning calorimetry (DSC) and thermogravimetric analysis (TGA) were performed on lithium salt, neat ILs and the corresponding electrolytes.

2.2.1. Differential Scanning Calorimetry (DSC)

The thermal analysis of all samples was investigated using a Setaram DSC 131 apparatus. A weighed sample of 5.0 ± 1 mg was placed in a sealed stainless crucible. A standard heating rate of 5 °C.min^{-1} was applied from 30 up to 650 °C under 50 mL.min^{-1} of nitrogen. The start and the onset temperatures were determined in order to assess the thermal stability. T_{start} is the temperature at which the sample starts to lose some mass and T_{onset} was determined from the step tangent method. Also, the heat of decomposition of each sample was calculated based on the curve integration.

2.2.2. Thermogravimetric analysis (TGA)

The thermogravivetric analysis scans were collected on a Mettler Toledo TGA DSC 1. The instrument was calibrated using indium, zinc and aluminum samples. Experiments were carried out in 40 µL aluminum pans, filled and sealed in an argon-filled glove box. Samples of 10 ± 3 mg were heated under an argon flow of 30 mL.min^{-1}. Two types of TGA experiments were investigated. The first one called *dynamic experiment* was carried out using a temperature increase from 30 to 500 °C at 5 °C.min^{-1} heating rate. The onset temperature (T_{onset}) was determined from the step tangent method.[29, 34, 41, 42] The start temperature (T_{start}) is the temperature at which the sample starts to lose some mass[29] and was defined as the temperature at which the first derivative of the weight loss *vs.* time curve is $|dm/dT| > 10^{-4}$ %.s^{-1}. The associated uncertainty was 5 °C and the definitions are illustrated in Figure 1. The second experiment, called *isotherm experiment*, consisted in a temperature increase from 30 to the selected temperature, *e.g.* 350 °C, at 5 °C.min^{-1} heating rate, followed by a plateau of 4 or 15 h at *e.g.* 350 °C. The slope of the curve, representing the mass loss rate, was determined between 2 and 10 h. For each experiment an argon background was subtracted.

2.2.3. Thermal treatment of electrolytes

3 mL of the electrolytes $[C_1C_4Im][Li][NTf_2]$ or $[PYR_{14}][Li][NTf_2]$ were introduced in a schlenk and dried under high vacuum (10^{-5} mbar) overnight before the experiment. The solution was heated by a tubular oven at 10 °C.min^{-1} heating rate up to 350 °C. It was kept for 2 h at this temperature while the pressure of the emitted gases was measured by a capacitance diaphragm gauge. At the end, the gas phase was analysed by infrared spectroscopy (FT-IR), by gas chromatography (GC) and by GC coupled with mass spectroscopy (GC-MS). The liquid phase was analysed by ^{1}H, ^{13}C, ^{19}F and ^{7}Li liquid NMR spectroscopy and by mass spectroscopy.

FT-IR spectra were recorded in a Nicolet 5700 spectrophotometer. 32 scans were accumulated for each spectrum (resolution 1 cm^{-1}). A 25 m PORA BOND Q column was used to separate the products that were then analysed in the online GC-MS (Agilent GC 6850 MS 5975C). GC analyses were achieved on KCl alumina column.

2.3. Burning behaviour in fire conditions

The fire behaviour of the ILs and the electrolytes were determined using the Tewarson calorimeter also covered under the name of Fire Propagation Apparatus (FPA) by different standards, namely NFPA 287[43] and ISO 12136.[44] This equipment allows getting information about ignitability, fire propagation potential and thermal and chemical threats in fire condition. It has been described in detail by Brohez et al.[45, 46] and has recently been used to investigate the combustion hazard profiles of several neat ILs.[47] The theoretical energies of combustion (lower heating values or LHV) were measured in an oxygen bomb calorimeter Model 1108P, Oxygen Combustion Bomb, Parr Instrument Co., Moline, Illinois.

In this work, approximately 55 g of sample were poured into a glass sample holder. An external heat flux of 50 kW.m^{-2} simulating fire environment or external thermal stress was set in operation by four infrared heaters in an air-flushed jacket. Thus, the sample was heated to a temperature where its vapours or flammable decomposition products can be ignited by an electric spark. The heat release rate (HRR) can be calculated by applying fire calorimetry laws, such as the oxygen consumption (OC)[48] or the carbon dioxide generation (CDG).[49] The mass loss rates as well as the fire effluent concentrations were measured *in situ*. The related emission yields (mass ratio of pollutants per burnt product) were then deduced allowing an evaluation of fire toxicity issues. In order to maintain self-sustained combustion, after ignition the external flux was diminished to 25 kW.m^{-2}.[47]

3. Results and discussion

Neat ILs and the corresponding electrolytes were studied under thermal abuse conditions such as overheating and combustion. The thermal stability was firstly determined by DSC and TGA studies. Then long term stability was studied by TGA, and a specific setup was used to analyse the decomposition products. Finally the electrolyte behaviour was tested in fire conditions, along with the identification and quantification of the emitted compounds.

3.1. DSC

The DSC results of lithium salt, ILs and their corresponding electrolytes are shown in Figure 2. All liquid samples remained stable up to 400 °C (using the start temperature) while solid $LiNTf_2$ started to decompose at 355 °C. Onset temperatures showed the same tendency, respectively at 450 °C and 396 °C. In the case of $LiNTf_2$, a two-step decomposition reaction occurred at rather high temperatures 355 - 420 °C and 500 - 650 °C, whereas for the neat ILs and their corresponding electrolytes a single-step was observed. Reaction enthalpies obtained by integrating the exothermic peaks are given in Table 1. As can be seen from this table, $[C_1C_4Im][NTf_2]$ and $[PYR_{14}][NTf_2]$ showed an exothermic peak corresponding to reaction heats of respectively 1579 $J.g^{-1}$ and 1644 $J.g^{-1}$. The electrolytes showed slightly inferior reaction enthalpies (1406 $J.g^{-1}$ for $[C_1C_4Im][Li][NTf_2]$ and 1470 $J.g^{-1}$ for $[PYR_{14}][Li][NTf_2]$), even if in the case of $[PYR_{14}][Li][NTf_2]$ the addition of lithium salt increased the height of the exothermic peak. These results suggest that the addition of $LiNTf_2$ lead to an improvement in thermal stability, which was not predictable from the decomposition temperatures of neat products.

3.2. Thermogravimetric analyses (TGA)

Because of the extremely low volatility of most ILs, their liquid range upper limit is defined by their decomposition temperature (T_d).[20] In the literature, the T_d is generally obtained from thermogravimetric analysis (TGA). However, several parameters can vary and influence T_d value, like the heating rate, the gas nature and flow rate, the nature of the pan, the apparatus and the purity of the sample. Hence results can be compared only if all the experimental parameters are the same.[27, 29, 42, 50-55] Furthermore TGA reveals only degradation due to the formation of volatile species, implying that degradation occurring without mass loss is not visible. Typically, the onset temperature (T_{onset}) is used to define the stability of ILs, and is determined from the step tangent method.[29, 34, 41, 42] Unfortunately, the values obtained from this method for a same IL can differ of more than 100 °C from one study to another, *e.g.* the

T_d of $[C_1C_4Im][NTf_2]$ varies from 275[56] to 461 °C.[57] In literature, authors are now well aware of this when presenting TGA results and it is admitted that the thermal decomposition could occur well before T_{onset}.[27]

3.2.1. Dynamic TGA

The TGA spectra of $[C_1C_4Im][NTf_2]$, $[PYR_{14}][NTf_2]$, $LiNTf_2$ and their corresponding electrolytes were reported in Figure 3, and the experimentally determined T_{start} and T_{onset} in Table 2. All these products were thermally stable up to 300 °C, in line with the literature.[29, 51, 58, 59] The observed decomposition occurred in one step from 330 to 480 °C, leading to residual masses of 16 % for $[C_1C_4Im][NTf_2]$ and $[C_1C_4Im][Li][NTf_2]$, 5 % for $[PYR_{14}][NTf_2]$, 8 % for $[PYR_{14}][Li][NTf_2]$ and 12 % for $LiNTf_2$ salt.

In Table 2, all ILs and electrolytes exhibit a T_{onset} ~ 428 ± 6 °C revealing no significant difference between them. The T_d values determined by T_{start} were inferior and showed that the neat $[PYR_{14}][NTf_2]$ decomposed ~ 100 °C before $[C_1C_4Im][NTf_2]$ (277 *vs.* 360 °C). This trend was confirmed for their electrolytes, for which the T_d difference was ~ 20 °C (339 *vs.* 357 °C). $LiNTf_2$ was the least stable product, with a T_{onset} of 369 °C and a T_{start} of 298 °C. The addition of $LiNTf_2$ to the ILs did not have a significant effect on the T_d (< 7 °C) except for T_{start} of $[PYR_{14}][NTf_2]$ (+ 60 °C).

DSC and dynamic TGA results confirm that $[C_1C_4Im][NTf_2]$ was more stable than $[PYR_{14}][NTf_2]$, and that this tendency was similar for the derived electrolytes. The use of T_{start} was more relevant than T_{onset}, in order to avoid misleading results.[60]

3.2.2. Long term isothermal TGA

The dynamic TGA can be used as a screening method but long term stability is required for industrial applications. In order to afford information on the maximum operating temperature (T_{op}), isothermal long term TGA can be performed. Indeed T_{op} is generally significantly lower than T_d obtained from dynamic TGA and DSC experiments.[27]

For neat ILs and electrolytes, the temperatures between 300 and 400 °C corresponding to T_{start} ± 50 °C were screened (Figures 4 and 5). For all these products no detectable mass loss was observed at 300 °C after 4 h. For $[C_1C_4Im][NTf_2]$ the mass loss was 14 % after 4 h at 350 °C. At 375 and 400 °C, the mass decreased faster to reach mass loss of 46 and 89 % respectively in 4 h. For $[PYR_{14}][NTf_2]$, a fast decrease was observed after 4 h for temperatures superior to 325 °C, to reach mass loss of 17 % at 325 °C, 30 % at 350 °C, 52 %

at 375 °C and 94 % after only 1 h at 400 °C. Obviously $[C_1C_4Im][NTf_2]$ decomposed at higher temperatures and slower than $[PYR_{14}][NTf_2]$. For both electrolytes, whatever the temperature, the mass loss was lower than for the corresponding pure ILs (Figure 6). Yet, at 400 °C, the mass loss reached 80 % in 170 min for $[C_1C_4Im][Li][NTf_2]$ instead of 70 min for $[C_1C_4Im][NTf_2]$, and 80 % in 150 min for $[PYR_{14}][Li][NTf_2]$ instead of 30 min for $[PYR_{14}][NTf_2]$. Generally the mass loss rates were lower in the case of the electrolytes.

Then longer isothermal TGA experiments were performed (15 h at 250 and 350 °C) on ionic liquids and electrolytes. At 250 °C no appreciable thermal decomposition of the neat ILs occurred even after 15 h (Figure 7). At 350 °C, a temperature significantly inferior to T_{onset}, a significant mass loss was observed (Figure 8) as reported for other neat ILs.[61] For $[C_1C_4Im][NTf_2]$ and $[C_1C_4Im][Li][NTf_2]$ a similar monotonous decrease was observed, with respective slopes of 3,5 and 3,3 $\%.h^{-1}$, and reaching respectively 50 and 47 % mass loss. For $[PYR_{14}][NTf_2]$ the decomposition occurred at two different rates, the first until 8 h at 7.9 $\%.h^{-1}$ reaching 60 % mass loss, and a second with a slope of 2.8 $\%.h^{-1}$ affording a mass loss of 86 %. For $[PYR_{14}][Li][NTf_2]$, the same evolution was apparent but with lower rates. The first curve had a slope of 5.5 $\%.h^{-1}$ corresponding to a mass loss of 43 %, and the second one had a slope of 3.0 $\%.h^{-1}$ yielding residual mass of 68 %. The highest stability of imidazolium-based solutions compared to pyrrolidinium was confirmed and emphasised. Indeed $[PYR_{14}][NTf_2]$ decomposed two times faster than $[C_1C_4Im][NTf_2]$ in these analogous conditions (7.9 *vs.* 3.5 $\%.h^{-1}$). (Table 3)

3.3. Thermal treatment of electrolytes $[C_1C_4Im][Li][NTf_2]$ and $[PYR_{14}][Li][NTf_2]$

TGA reveals only decomposition due to the formation of volatile species, implying that degradation occurring without mass loss is not visible. Moreover, the temperature of 350 °C seemed appropriate to analyse the decomposition products as a mass loss comprised between 5 and 10 % was expected (Figure 5). So in this part, the long term stability (350 °C during 2 h) on larger quantities of electrolytes was studied. We aimed to quantify and characterise the volatiles and the residual liquid phase. From the TGA results *vide supra*, a measurable decomposition of the electrolytes occurred in these conditions.

3 mL of the solution of ILs containing 1 $mol.L^{-1}$ of $LiNTf_2$ were introduced in a specific setup described in Figure SI-3, and dried under high vacuum (10^{-5} mbar) overnight before the experiment. The reactor was closed and the solution was heated at 10 °C.min^{-1} heating rate, up to 350 °C. It was kept for 2 h at this temperature while the evolution of the pressure was

measured. The gaseous phase was then analysed by IR, GC and GC-MS, and the residual liquid phase by solution NMR and by GC-MS.

3.3.1. Gas phase analysis

After 2 h the pressure levels of the gas phase were respectively 17 *vs* 50 mbars for $[C_1C_4Im][Li][NTf_2]$ and $[PYR_{14}][Li][NTf_2]$, with expected mass losses of 9 % and 6 % as determined from the long term TGA experiments. The results are shown in Figure 9 and the slopes of the curves were respectively 0.18 $mbar.min^{-1}$ and 0.46 $mbar.min^{-1}$ for $[C_1C_4Im][Li][NTf_2]$ and $[PYR_{14}][Li][NTf_2]$. The discrepancy between the two electrolytes was even higher (ratio between the slopes of 2.5) than the one found by long term TGA experiments (ratio of 1.7).

For both electrolytes the gas phases were mainly constituted of butene isomers, identified by GC and GC-MS as trans-butene (5.7 min), 1-butene (5.85 min) and cis-butene (6.01 min) (Figure 10). They could result from the cleavage of the butyl-N bond of the cationic ring. Similarly (from the cleavage of the methyl-N bond), methane was detected at 1.31 min for both electrolytes. GC and GC-MS analyses evidenced the presence of traces of pentene isomers, ethane, ethene, propene, butane (Figure SI-4). Some differences in the nature of hydrocarbons were observed. This could be due to their origin, as for $[C_1C_4Im][Li][NTf_2]$ hydrocarbons come only from the alkyl chains, but for $[PYR_{14}][Li][NTf_2]$ they also come from the pyrrolidinium ring (Figure SI-5).[27, 51, 53, 62] Some compounds resulting from the anion decomposition such as CF_3H (1.77) and $HN(CF_3)(SO_2CF_3)$ (3.7 min) were also detected. Note that the gaseous phase was acidic (pH ~ 2).

The IR spectra of this gaseous phase (Figure SI-6) showed the characteristic bands of these alkanes and alkenes: $\nu(C\text{-}H_{sp3})$ at 2800-3000 cm^{-1}, to $\nu(C\text{-}H_{sp3})$ at 3038 cm^{-1}, to $\delta(C\text{-}H)$ at 1477 cm^{-1} and to $\nu(C{=}C)$ at 1649 cm^{-1}. The sharp peaks at 1376 and 1155 cm^{-1} could be assigned to $\nu(S{=}O)$ function.

3.3.2. Liquid phase analysis

After 2 h at 350 °C, the non-coloured transparent initial electrolytes turned to dark yellow to brown (Figure 11). No suspension or apparent increases of the viscosities were observed after the thermal treatment, and few changes were detected by ^{1}H and ^{13}C solution NMR (Figure SI-7).

The comparison of ESI^+ MS spectra of the electrolytes before and after thermal treatment at 350 °C indicated the presence of imidazolium and pyrrolidinium fragments in the thermally treated solutions (Table 4). These species resulted from alkyl chain cleavage or redistribution.[27, 57, 63] In the ESI^- MS spectra, fragments resulting from $[NTf_2]$ fragmentation have been detected (Table 4). Note that the ESI^+ MS spectra of neat imidazolium and pyrrolidinium ILs treated at 220 °C for 5 h exhibited only fragments resulting from the cleavage of the hydrocarbon chain, and no species resulting from alkyl chain redistribution.[64] Here the redistribution showed a chemical evolution of the nature of the cation ring occurring at constant weight.

In conclusion, these different thermal experiments confirmed that $[C_1C_4Im][NTf_2]$ was thermally more stable than $[PYR_{14}][NTf_2]$, in agreement with the literature.[31, 50] This result could be related to the presence of a strained five membered cycle in $[PYR_{14}]$ cation inducing an easy ring opening.[50] $LiNTf_2$ exhibited a lower T_d than both ILs (T_{start} of 298 °C). However its dissolution into ILs had a positive effect on their thermal stability, especially in the case of $[PYR_{14}][NTf_2]$. This could be related to the fact that the dissolution of $LiNTf_2$ in an IL sharing the same anion $[NTf_2]^-$ induced a restructuration of the anions around $[Li]^+$ cations, resulting in an increase of the coordination number of $[Li]^+$. Simulation and spectrometry results proved that $[Li]^+$ were linked to two to four $[NTf_2]^-$ anions through strong oxygen - lithium bonds.[65-67] These $[Li(NTf_2)_n]^{(n-1)-}$adducts[68, 69] must have a higher thermal stability than solid $LiNTf_2$. Note that the nature of the liquid and gas phases indicated that after 2 h both anion and cation started to decompose. Some of the characterised decomposition products were already suggested either theoretically[41] or experimentally.[62, 70, 71]

3.4. Fire Propagation Apparatus tests

3.4.1. Heat release rate (HRR) profiles

The results of combustion experiments performed in the Tewarson calorimeter on the ILs $[C_1C_4Im][NTf_2]$ and $[PYR_{14}][NTf_2]$ and on the electrolytes $[C_1C_4Im][Li][NTf_2]$ and $[PYR_{14}][Li][NTf_2]$ are summarised in Table 5, and the heat release rate profiles are shown in Figure 12. The theoretical energy of combustion of $LiNTf_2$ confirmed that the salt was not combustible as the gross heat of combustion obtained was 2.69 $MJ.kg^{-1}$. The neat ILs and their corresponding electrolytes showed good resistance to ignition under an external heat flux of 50 $kW.m^{-2}$, simulating fire conditions. The ignition delays of $[C_1C_4Im][NTf_2]$ and

$[PYR_{14}][NTf_2]$ were respectively 5.9 min and 4.6 min, after application of the mentioned external heat flux. These values, compared to phosphonium based IL $[P_{6,6,6,14}][NTf_2]$ (ignition delay of 4.5 min),[47] highlighted the highest resistance to the ignition of $[C_1C_4Im][NTf_2]$, and the role of the cation in flammability. The combustion behaviour of ILs was also really specific to the nature of anions.[47, 72] As an example, for a same imidazolium-based cation, a general trend of NTf_2 > OTf > BF_4 > $MeSO_3$ > $EtOSO_3$ > DCA was observed when looking which anion released the highest heat.

The ignition delay of $[PYR_{14}][NTf_2]$ was really high compared to flammable carbonates mixtures ones (commercial solvents for electrolytes), that were inferior to 50 sec, with half the value of external heat flux (25 $kW.m^{-2}$).[6] But $[PYR_{14}][NTf_2]$ ignition delay was shorter as compared to $[C_1C_4Im][NTf_2]$.

The ignition times of the electrolytes $[C_1C_4Im][Li][NTf_2]$ and $[PYR_{14}][Li][NTf_2]$ were 4.9 min and 5.5 min respectively. It indicated that the addition of the Li salt acts as a flame retardant for the $[PYR_{14}][Li][NTf_2]$. Contrarily it facilitates the combustion with $[C_1C_4Im][Li][NTf_2]$. From a combustibility viewpoint, the addition of the lithium salt in the solutions decreased the overall complete heats of combustion from some 19 % in both cases (as determined from data in Table 5). These results were quite in line with overall decrease of theoretical heating value available in the mixtures. The drop in effective energy release was less important in the case of $[C_1C_4Im][NTf_2]$ (23 %) as compared to $[PYR_{14}][NTf_2]$ (35 %).

The heat release rate profiles were quite similar for $[PYR_{14}][NTf_2]$ and $[PYR_{14}][Li][NTf_2]$ (with a peak of 475 $kW.m^{-2}$ and 425 $kW.m^{-2}$, respectively), showing a plateau throughout the combustion. By contrast, in the case of $[C_1C_4Im][NTf_2]$, the addition of the salt significantly modified the corresponding HRR profile after the first intermediate peak. Indeed a sharp secondary peak around time equal 7.6 min and reaching 775 $kW.m^{-2}$ was observed, resulting in accelerated second phase combustion. It revealed that the combustion of $[C_1C_4Im][Li][NTf_2]$ leads to combustible decomposition products. A similar peak of 475 $kW.m^{-2}$ was observed for the neat $[C_1C_4Im][NTf_2]$ near 9.3 min. Furthermore the combustion of $[C_1C_2Im]$ cation associated to different anions such as DCA, OTf, $MeSO_3$ or $EtOSO_3$ exhibit the same heat flow profile the same profile (appearance of a peak in the reaction medium)[47]. This unusual curve evolution observed for imidazolium-based ILs could be due to the presence of acidic C - H bonds of imidazolium cations, easily converted into NHC - carbenes under thermal or basic conditions.[73-75] This inherent reactivity could explain

the presence of a second phase combustion and the acceleration of the thermal decomposition of $[C_1C_4Im][Li][NTf_2]$ in the presence of lithium salt.

3.4.2. Toxicity of emissions

The combustion efficiency of a product can be estimated from the quantity of CO, total hydrocarbons (THCs) and soots. Indeed, lower combustion efficiency generally gives higher yields of these partially oxidised species. The combustion efficiencies of studied ILs was lower compared to carbonate solvents used in conventional lithium-ion batteries (close to 100 % in the case of fuel lean conditions, due to presence of oxygen atoms in the molecules).[6, 76]

The fire induced toxicity was also investigated in terms of emission factors of asphyxiant (HCN, CO) and irritant (NO_x, SO_2, and HF) gases. The emission factor is defined as the amount of pollutant emitted per mass unit of burned product. The amount of HCN released in the combustion of the electrolytes increased in comparison to the corresponding neat ILs (Table 6).

The combustion of ionic liquids was very specific to the nature of the anion and cation concerned. As an example, among the tested ionic liquids the formation of HCN and HF was found to be higher for DCA and NTf_2 anions respectively.[47] In addition, in the same study, heat release rates profiles were specific to each tested IL and were more versatile as compared to conventional liquid fires. In our case the combustion of $[PYR_{14}][Li][NTf_2]$ released less unburned carbon than $[C_1C_4Im][Li][NTf_2]$. Thus its amount of CO decreased as compared to parent ILs but still was higher than $[C_1C_4Im][Li][NTf_2]$ (25.1 $mg.g^{-1}$ *vs.* 21.6 $mg.g^{-1}$). Also, the emission asphyxiant gases were very high for both electrolytes, in particular the value exceeded was close to 295 $mg.g^{-1}$ of HF and 353 $mg.g^{-1}$ of SO_2 for the $[C_1C_4Im][Li][NTf_2]$. It appears that the emission of flammable compounds was related to the cation nature, whereas the anion produces toxic species.

The mass balance was also checked by performing combustion residues analysis of all tested samples (see SI-8). As can be seen, these results confirmed the mass conservation of hetero-atoms with high conversion efficiencies, which showed the smooth running of the apparatus.

4. Conclusion

Ionic liquids $[C_1C_4Im][NTf_2]$ and $[PYR_{14}][NTf_2]$ along with the electrolytes $[C_1C_4Im][Li][NTf_2]$ and $[PYR_{14}][Li][NTf_2]$ showed high thermal stabilities. From dynamic

DSC and TGA experiments, the products were stable up to 350 °C. Onset temperatures did not reveal any difference between the four solutions, but start temperatures (based on the derivative) showed that imidazolium cations form more stable ILs than pyrrolidinium. The addition of lithium salt clearly stabilised the solutions. Isotherm experiments at 350 °C confirmed and emphasised these trends.

During the combustion, all the solutions were very weakly combustible, especially compared to the current electrolytes (at least five times more resistant to ignition). Lithium salt has controversial effect on thermal stability, as it acts as flame retardant for $[PYR_{14}][Li][NTf_2]$ but facilitates the combustion with $[C_1C_4Im][Li][NTf_2]$. From a combustibility viewpoint, the addition of the lithium salt in the solutions decreased the overall complete heats of combustion. Flammable gases were emitted due to cation decomposition, and the anion decomposition formed toxic effluents.

These electrolytes exhibited good resistance to thermal stress, but fire induced toxicity can be an issue in case of an accidental fire scenario; thus it must be assessed on a case by case approach.

Acknowledgements

The authors wish to thank O. Boyron for the help with the TGA measurements and K. Szeto for the GC-MS experiments from C2P2. We thank F. Albrieux, C. Duchamp and N. Henriques, from the Centre Commun de Spectrométrie de Masse (CCSM) of Université Lyon 1, for the assistance and access to the mass spectrometry facility. Special thanks are addressed to Jean-Pierre Bertrand for having conducted the experiments on the Tewarson calorimeter. This work was performed, in partnership with the SAS PIVERT, within the frame of the French Institute of Excellence in the field of Low-Carbon Energies (IEED) P.I.V.E.R.T. (www.institut-pivert.com) selected as an Investment for the Future ("Investissements d'Avenir"). This work was supported, as part of the Investments for the Future, by the French Government under the reference ANR-001.

References

1. C. J. Barnhart and S. M. Benson, *Energy Environ. Sci.*, 2013, **6**, 1083-1092.
2. R. S. Kühnel, N. Böckenfeld, S. Passerini, M. Winter and A. Balducci, *Electrochim. Acta*, 2011, **56**, 4092-4099.
3. A. Guerfi, M. Dontigny, P. Charest, M. Petitclerc, M. Lagacé, A. Vijh and K. Zaghib, *J. Power Sources*, 2010, **195**, 845-852.

4. *World Hybrid Electric and Electric Vehicle Lithium-ion Battery Market*, Frost & Sullivan (subscription required), http://www.frost.com (accessed September 24, 2013) 2009.
5. Y. S. Yun, J. H. Kim, S. Y. Lee, E. G. Shim and D. W. Kim, *J. Power Sources*, 2011, **196**, 6750-6755.
6. G. G. Eshetu, S. Grugeon, S. Laruelle, S. Boyanov, A. Lecocq, J. P. Bertrand and G. Marlair, *Phys. Chem. Chem. Phys.*, 2013, **15**, 9145-9155.
7. C. L. Campion, W. Li and B. L. Lucht, *J. Electrochem. Soc.*, 2005, **152**, A2327-A2334.
8. D. R. MacFarlane, N. Tachikawa, M. Forsyth, J. M. Pringle, P. C. Howlett, G. D. Elliott, J. H. Davis, M. Watanabe, P. Simon and C. A. Angell, *Energy Environ. Sci.*, 2013, **(in press)**.
9. M. A. Navarra, *MRS Bull.*, 2013, **38**, 548-553.
10. B. Scrosati and J. Garche, *J. Power Sources*, 2010, **195**, 2419-2430.
11. M. Armand, F. Endres, D. R. MacFarlane, H. Ohno and B. Scrosati, *Nat. Mater.*, 2009, **8**, 621-629.
12. M. Galinski, A. Lewandowski and I. Stepniak, *Electrochim. Acta*, 2006, **51**, 5567-5580.
13. *China Pat.,* US 2013/0029232 A1, 2013.
14. *Belgium Pat.,* EP2410603A1, 2012.
15. A. Balducci, S. S. Jeong, G. T. Kim, S. Passerini, M. Winter, M. Schmuck, G. B. Appetecchi, R. Marcilla, D. Mecerreyes, V. Barsukov, V. Khomenko, I. Cantero, I. De Meatza, M. Holzapfel and N. Tran, *J. Power Sources*, 2011, **196**, 9719-9730.
16. *France Pat.,* WO 2009/007540, 2009.
17. *Japan Pat.,* WO 2007/088677, 2007.
18. H. Srour, H. Rouault and C. C. Santini, *J. Electrochem. Soc.*, 2013, **160**, A781-A785.
19. A. Lewandowski and A. Swiderska-Mocek, *J. Power Sources*, 2009, **194**, 601-609.
20. P. Wasserscheid and T. Welton, *Ionic liquids in synthesis. 1st Edition*, WILEY-VCH, Weinheim, 2003.
21. D. M. Fox, J. W. Gilman, A. B. Morgan, J. R. Shields, P. H. Maupin, R. E. Lyon, H. C. De Long and P. C. Trulove, *Ind. Eng. Chem. Res*, 2008, **47**, 6327-6332.
22. M. Smiglak, W. M. Reichert, J. D. Holbrey, J. S. Wilkes, L. Y. Sun, J. S. Thrasher, K. Kirichenko, S. Singh, A. R. Katritzky and R. D. Rogers, *Chem. Commun.*, 2006, 2554-2556.
23. B. Garcia, S. Lavallee, G. Perron, C. Michot and M. Armand, *Electrochim. Acta*, 2004, **49**, 4583-4588.
24. A. O. Diallo, C. Len, A. B. Morgan and G. Marlair, *Separation and Purification Technology*, 2012, **97**, 228-234.
25. H.-J. Liaw, C.-C. Chen, Y.-C. Chen, J.-R. Chen, S.-K. Huang and S.-N. Liu, *Green Chem.*, 2012, **14**, 2001-2008.
26. *Globally Harmonized System of Classification and Labelling of Chemicals, 4th revised edition*, New York and Geneva, 2011.
27. C. Maton, N. De Vos and C. V. Stevens, *Chem. Soc. Rev.*, 2013, **42**, 5963-5977.
28. A. Seeberger, A.-K. Andresen and A. Jess, *Phys. Chem. Chem. Phys.*, 2009, **11**, 9375-9381.
29. C. P. Fredlake, J. M. Crosthwaite, D. G. Hert, S. Aki and J. F. Brennecke, *J. Chem. Eng. Data*, 2004, **49**, 954-964.
30. P. Andersson, P. Blomqvist, A. Lorén and F. Larsson, *Investigation of fire emissions from Li-ion batteries*, 2013.
31. C. S. Stefan, D. Lemordant, P. Biensan, C. Siret and B. Claude-Montigny, *J. Therm. Anal. Calorim.*, 2010, **102**, 685-693.
32. P. S. Kulkarni, L. C. Branco, J. G. Crespo, M. C. Nunes, A. Raymundo and C. A. M. Afonso, *Chem. Eur. J.*, 2007, **13**, 8478-8488.
33. N. Papaiconomou, J. Salminen, J.-M. Lee and J. M. Prausnitz, *J. Chem. Eng. Data*, 2007, **52**, 833-840.
34. D. M. Blake, L. Moens, D. Rudnicki and H. Pilath, *J. Sol. Energy Eng.*, 2006, **128**, 54-57.
35. S. A. Forsyth, S. R. Batten, Q. Dai and D. R. MacFarlane, *Aust. J. Chem.*, 2004, **57**, 121-124.
36. H. L. Ngo, K. LeCompte, L. Hargens and A. B. McEwen, *Thermochim. Acta*, 2000, **357**, 97-102.

37. S. Passerini and G. B. Appetecchi, *MRS Bull.*, 2013, **38**, 540-547.
38. L. Magna, Y. Chauvin, G. P. Niccolai and J. M. Basset, *Organometallics*, 2003, **22**, 4418-4425.
39. P. Bonhote, A. P. Dias, N. Papageorgiou, K. Kalyanasundaram and M. Gratzel, *Inorg. Chem.*, 1996, **35**, 1168-1178.
40. H. Srour, H. Rouault, C. C. Santini and Y. Chauvin, *Green Chem.*, 2013, **15**, 1341-1347.
41. M. C. Kroon, W. Buijs, C. J. Peters and G.-J. Witkamp, *Thermochim. Acta*, 2007, **465**, 40-47.
42. M. E. Van Valkenburg, R. L. Vaughn, M. Williams and J. S. Wilkes, *Thermochim. Acta*, 2005, **425**, 181-188.
43. *NFPA 287: Standard Test Methods for Measurement of Flammability of Materials in Cleanrooms Using a Fire Propagation Apparatus (FPA)*, 2001.
44. *ISO 12136:2011 Reaction to fire tests, Measurement of material properties using a fire propagation apparatus*, 2011.
45. S. Brohez, G. Marlair and C. Delvosalle, *Fire Mater.*, 2006, **30**, 131-149.
46. S. Brohez, G. Marlair and C. Delvosalle, *Fire Mater.*, 2006, **30**, 35-50.
47. A.-O. Diallo, A. B. Morgan, C. Len and G. Marlair, *Energy Environ. Sci.*, 2013, **6**, 699-710.
48. C. Huggett, *Fire Mater.*, 1980, **4**, 61-65.
49. M. JE, *Physical Properties of Polymers Handbook. 2nd Revised edition.*, 2007.
50. R. E. Del Sesto, T. M. McCleskey, C. Macomber, K. C. Ott, A. T. Koppisch, G. A. Baker and A. K. Burrell, *Thermochim. Acta*, 2009, **491**, 118-120.
51. T. J. Wooster, K. M. Johanson, K. J. Fraser, D. R. MacFarlane and J. L. Scott, *Green Chem.*, 2006, **8**, 691-696.
52. D. M. Fox, J. W. Gilman, H. C. De Long and P. C. Trulove, *J. Chem. Thermodyn.*, 2005, **37**, 900-905.
53. K. J. Baranyai, G. B. Deacon, D. R. MacFarlane, J. M. Pringle and J. L. Scott, *Aust. J. Chem.*, 2004, **57**, 145-147.
54. M. Kosmulski, J. Gustafsson and J. B. Rosenholm, *Thermochim. Acta*, 2004, **412**, 47-53.
55. D. M. Fox, W. H. Awad, J. W. Gilman, P. H. Maupin, H. C. De Long and P. C. Trulove, *Green Chem.*, 2003, **5**, 724-727.
56. S. Holopainen, M. Nousiainen, J. Puton, M. Sillanpaa, U. Bardi and A. Tolstogouzov, *Talanta*, 2011, **83**, 907-915.
57. N. Meine, F. Benedito and R. Rinaldi, *Green Chem.*, 2010, **12**, 1711-1714.
58. J. Salminen, N. Papaiconomou, R. A. Kumara, J. M. Lee, J. Kerr, J. Newman and J. M. Prausnitz, *Fluid Phase Equilibr.*, 2007, **261**, 421-426.
59. H. Tokuda, K. Hayamizu, K. Ishii, M. Susan and M. Watanabe, *J. Phys. Chem. B*, 2005, **109**, 6103-6110.
60. M. E. Van Valkenburg, R. L. Vaughn, M. Williams and J. S. Wilkes, *Abstr. Pap. Am. Chem. S.*, 2002, **224**, U621-U622.
61. J. Salgado, M. Villanueva, J. J. Parajo and J. Fernandez, *J. Chem. Thermodyn.*, 2013, **65**, 184-190.
62. H. Ohtani, S. Ishimura and M. Kumai, *Anal. Sci.*, 2008, **24**, 1335-1340.
63. W. H. Awad, J. W. Gilman, M. Nyden, R. H. Harris, T. E. Sutto, J. Callahan, P. C. Trulove, H. C. DeLong and D. M. Fox, *Thermochim. Acta*, 2004, **409**, 3-11.
64. M. Nousiainen, A. Tolstogouzov, S. Holopainen, J. Jänis and M. Sillanpää, *Rapid Commun. Mass Sp.*, 2011, **25**, 2565-2569.
65. C. J. F. Solano, S. Jeremias, E. Paillard, D. Beljonne and R. Lazzaroni, *J. Chem. Phys.*, 2013, **139**.
66. A. Andriola, K. Singh, J. Lewis and L. Yu, *J. Phys. Chem. B*, 2010, **114**, 11709-11714.
67. O. Borodin, G. D. Smith and W. Henderson, *J. Phys. Chem. B*, 2006, **110**, 16879-16886.
68. J.-C. Lassegues, J. Grondin, C. Aupetit and P. Johansson, *J. Phys. Chem. A*, 2009, **113**, 305-314.
69. M. J. Monteiro, F. F. C. Bazito, L. J. A. Siqueira, M. C. C. Ribeiro and R. M. Torresi, *J. Phys. Chem. B*, 2008, **112**, 2102-2109.
70. G. Chatel, R. Pflieger, E. Naffrechoux, S. I. Nikitenko, J. Suptil, C. Goux-Henry, N. Kardos, B. Andrioletti and M. Draye, *ACS Sustainable Chem. Eng.*, 2013, **1**, 137-143.

71. M. Y. Keating, F. Gao and J. B. Ramsey, *J. Therm. Anal. Calorim.*, 2011, **106**, 207-211.
72. A. B. Morgan, *Interflam* 2010, **12**, 269–280
73. H. Yao, J. Zhang, Y. Zhang, H. Sun and Q. Shen, *Organometallics*, 2010, **29**, 5841-5846.
74. S. P. Nolan, *N-Heterocyclic carbenes in synthesis*, WILEY-VCH, Weinheim, 2006.
75. R. A. Olofson, J. S. Michelmay and W. R. Thompson, *J. Am. Chem. Soc.*, 1964, **86**, 1865-1866.
76. P. Ribiere, S. Grugeon, M. Morcrette, S. Boyanov, S. Laruelle and G. Marlair, *Energy Environ. Sci.*, 2012, **5**, 5271-5280.

Scheme 1: Typical components of current electrolytes

Figure 1: Determination of the onset temperature (T_{onset}) and the start temperature (T_{start}) for $[C_1C_4Im][NTf_2]$; 5 °C.min^{-1} heating rate, argon flow 30 mL.min^{-1}, aluminum sealed pan, 10 mg samples

Figure 2: DSC curves of $[C_1C_4Im][NTf_2]$, $[PYR_{14}][NTf_2]$, $[C_1C_4Im][Li][NTf_2]$, $[PYR_{14}][Li][NTf_2]$ and $LiNTf_2$; 5 °C.min^{-1} heating rate, nitrogen flow 50 mL.min^{-1}

Figure 3: Dynamic TGA of $[C_1C_4Im][NTf_2]$, $[PYR_{14}][NTf_2]$, $[C_1C_4Im][Li][NTf_2]$, $[PYR_{14}][Li][NTf_2]$, and $LiNTf_2$; 5 °C.min^{-1} heating rate from 30 to 500 °C, argon flow 30 mL.min^{-1}, aluminum sealed pan, 10 mg samples

Figure 4: Isotherm thermogravimetric analyses of $[C_1C_4Im][NTf_2]$ and $[PYR_{14}][NTf_2]$ between 300 °C and 400 °C for 4 h; argon flow 30 mL.min^{-1}, aluminum sealed pans, 10 mg samples.

Figure 5: Isotherm thermogravimetric analyses of $[C_1C_4Im][Li][NTf_2]$ and $[PYR_{14}][Li][NTf_2]$ between 300 °C and 400 °C for 4 h; argon flow 30 mL.min^{-1}, aluminum sealed pans, 10 mg samples

Figure 6: Isotherm thermogravimetric analyses of $[C_1C_4Im][NTf_2]$, $[PYR_{14}][NTf_2]$, $[C_1C_4Im][Li][NTf_2]$ and $[PYR_{14}][Li][NTf_2]$ at 325 °C and 400 °C for 4 h; argon flow 30 mL.min^{-1}, aluminum sealed pans, 10 mg samples

Figure 7: Long term thermogravimetric analyses of $[C_1C_4Im][NTf_2]$ and $[PYR_{14}][NTf_2]$ at 250 °C and 350 °C for 15 h; argon flow 30 mL.min^{-1}, aluminum sealed pans, 10 mg samples

Figure 8: Long term thermogravimetric analyses of 4 solutions and lithium salt at 350 °C for 15 h; argon flow 30 mL.min^{-1}, aluminum sealed pans, 10 mg samples

Figure 9: Evolution of the gas phase pressure during thermal treatment of $[C_1C_4Im][Li][NTf_2]$ and $[PYR_{14}][Li][NTf_2]$ during 2 h at 350 °C

Figure 10: Comparison of gas phase chromatograms of $[C_1C_4Im][Li][NTf_2]$ and $[PYR_{14}][Li][NTf_2]$ from GC-MS apparatus

Figure 11: Electrolytes before thermal treatment (left) and after 2 h at 350 °C: middle: $[PYR_{14}][Li][NTf_2]$, right: $[C_1C_4Im][Li][NTf_2]$

Figure 12: HRR profiles obtained by use of the Fire Propagation Apparatus (ISO:12136)

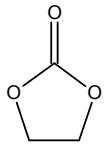

Ethylene carbonate (EC)

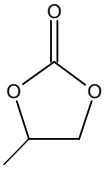

Propylene carbonate (PC)

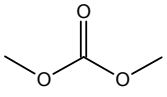

Dimethyl-carbonate (DMC)

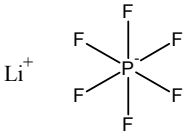

$LiPF_6$ lithium hexafluorophosphate

Scheme 1:

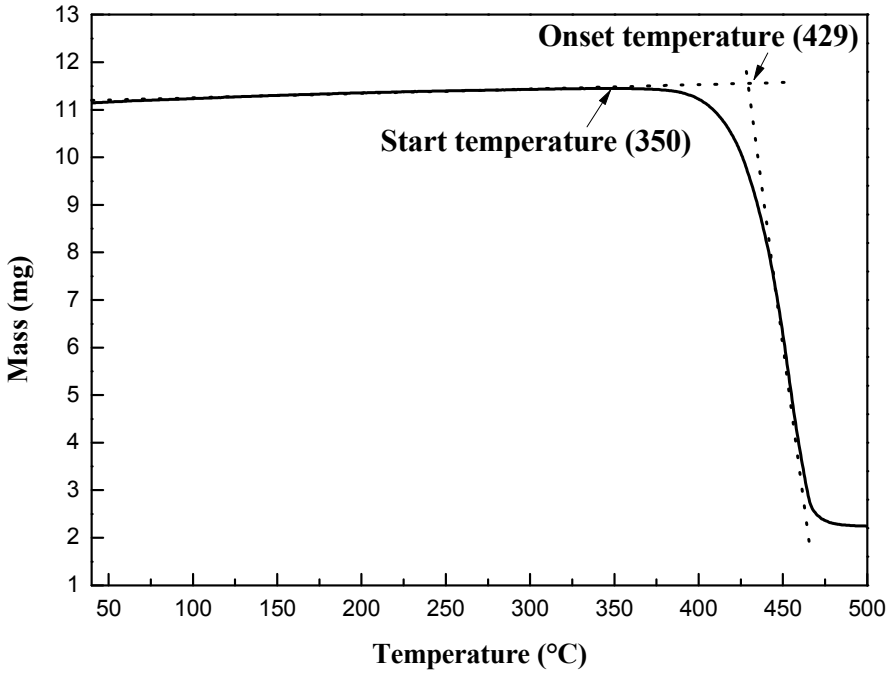
Onset temperature (429)
Start temperature (350)
Mass (mg)
Temperature (°C)
13
12
11
10
9
8
7
6
5
4
3
2
1
50
100
150
200
250
300
350
400
450
500

Figure 1:

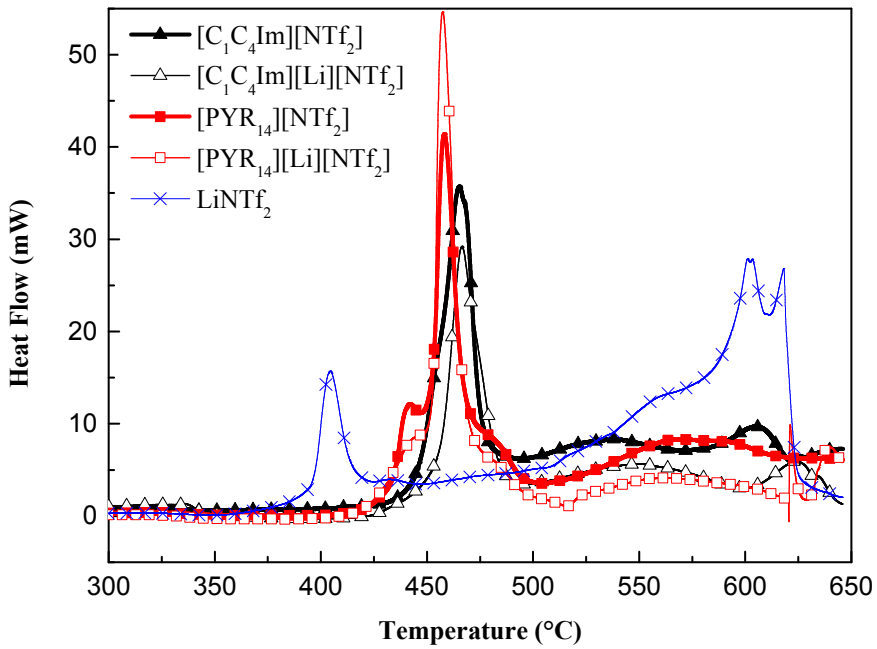
[C1C4Im][NTf2]
[C1C4Im][Li][NTf2]
[PYR14][NTf2]
[PYR14][Li][NTf2]
LiNTf2
Heat Flow (mW)
Temperature (°C)
0
10
20
30
40
50
300
350
400
450
500
550
600
650

Figure 2:

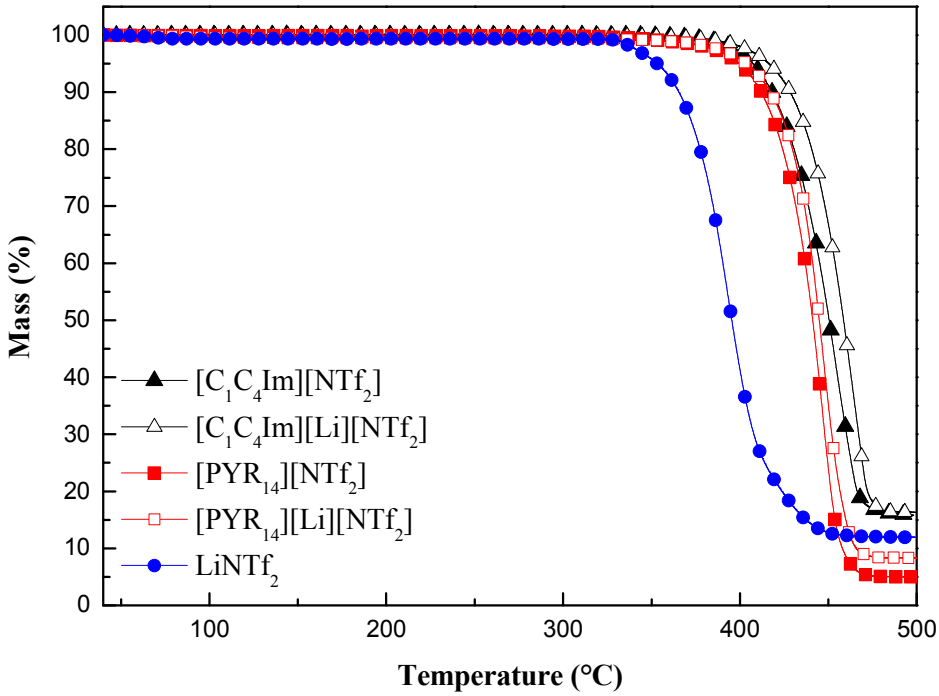
Mass (%)
Temperature (°C)
100
90
80
70
60
50
40
30
20
10
0
100
200
300
400
500
[C1C4Im][NTf2]
[C1C4Im][Li][NTf2]
[PYR14][NTf2]
[PYR14][Li][NTf2]
LiNTf2

Figure 3:

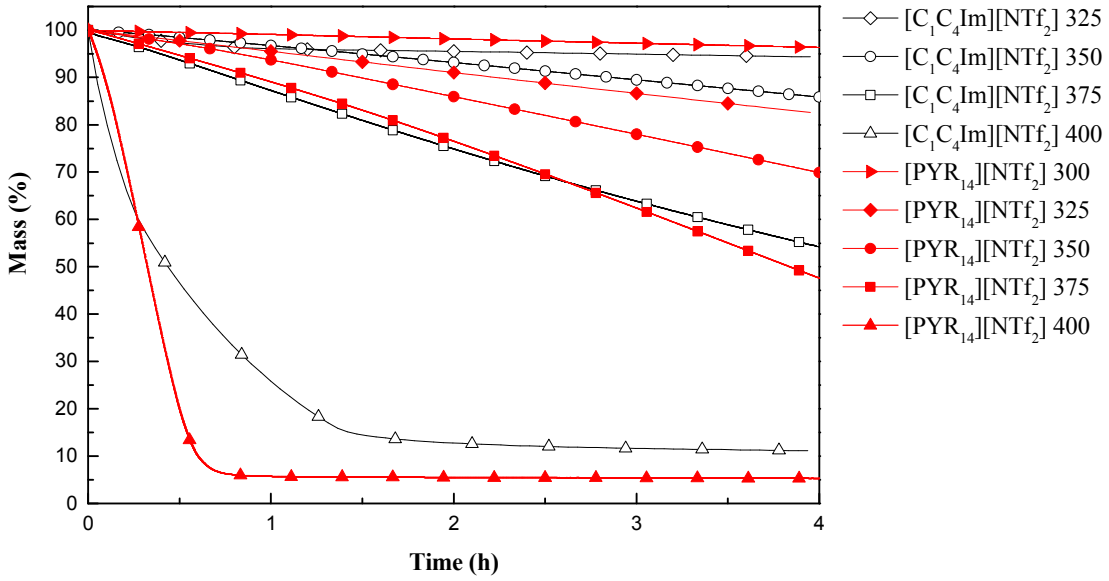
Mass (%)
Time (h)
0
10
20
30
40
50
60
70
80
90
100
0
1
2
3
4
[C1C4Im][NTf2] 325
[C1C4Im][NTf2] 350
[C1C4Im][NTf2] 375
[C1C4Im][NTf2] 400
[PYR14][NTf2] 300
[PYR14][NTf2] 325
[PYR14][NTf2] 350
[PYR14][NTf2] 375
[PYR14][NTf2] 400

Figure 4:

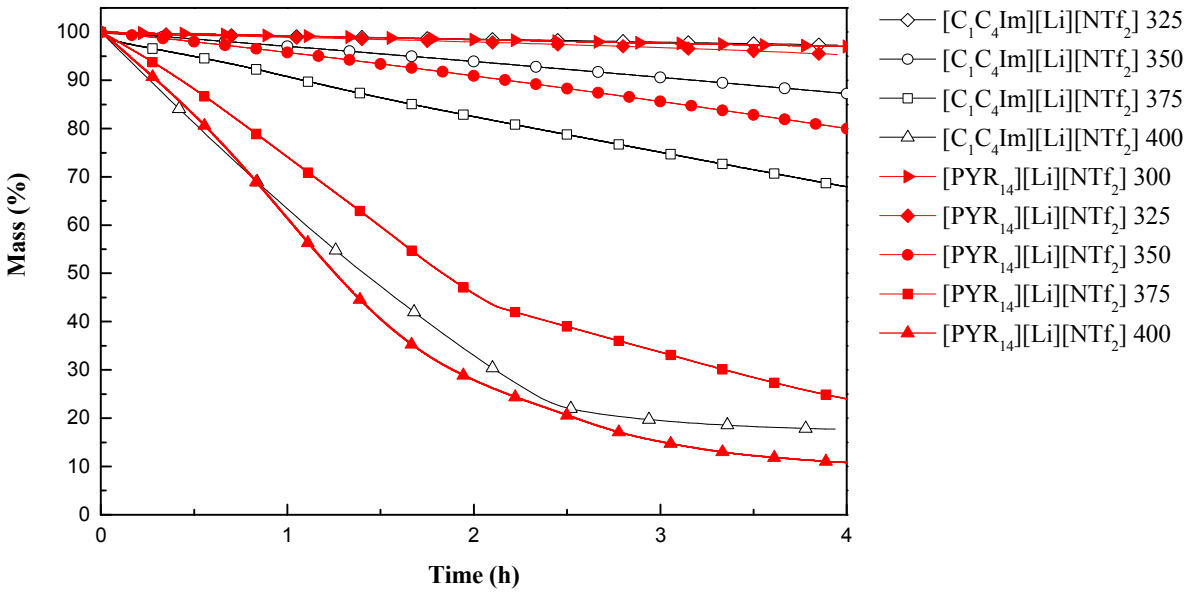
Mass (%)
Time (h)
0
10
20
30
40
50
60
70
80
90
100
0
1
2
3
4
[C1C4Im][Li][NTf2] 325
[C1C4Im][Li][NTf2] 350
[C1C4Im][Li][NTf2] 375
[C1C4Im][Li][NTf2] 400
[PYR14][Li][NTf2] 300
[PYR14][Li][NTf2] 325
[PYR14][Li][NTf2] 350
[PYR14][Li][NTf2] 375
[PYR14][Li][NTf2] 400

Figure 5:

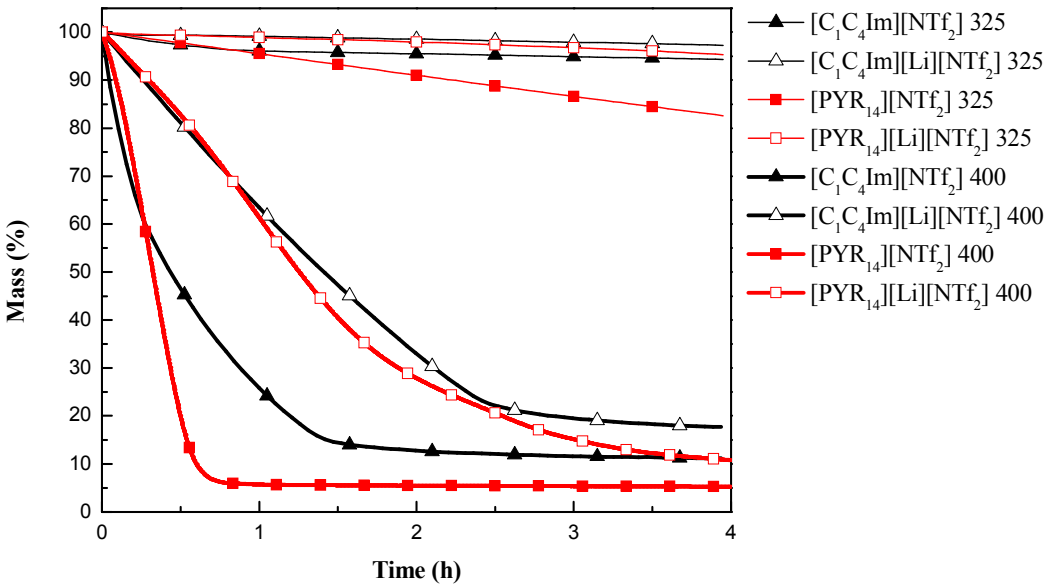
Mass (%)
Time (h)
0
10
20
30
40
50
60
70
80
90
100
0
1
2
3
4
[C1C4Im][NTf2] 325
[C1C4Im][Li][NTf2] 325
[PYR14][NTf2] 325
[PYR14][Li][NTf2] 325
[C1C4Im][NTf2] 400
[C1C4Im][Li][NTf2] 400
[PYR14][NTf2] 400
[PYR14][Li][NTf2] 400

Figure 6:

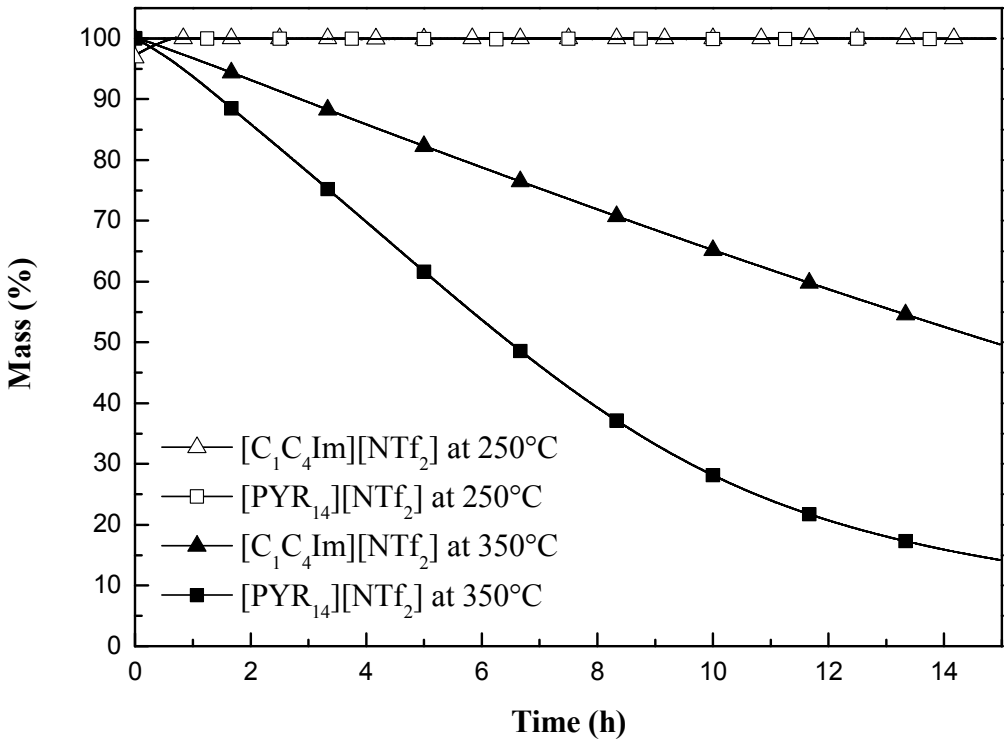
Mass (%)
Time (h)
[C1C4Im][NTf2] at 250°C
[PYR14][NTf2] at 250°C
[C1C4Im][NTf2] at 350°C
[PYR14][NTf2] at 350°C
0
10
20
30
40
50
60
70
80
90
100
0
2
4
6
8
10
12
14

Figure 7:

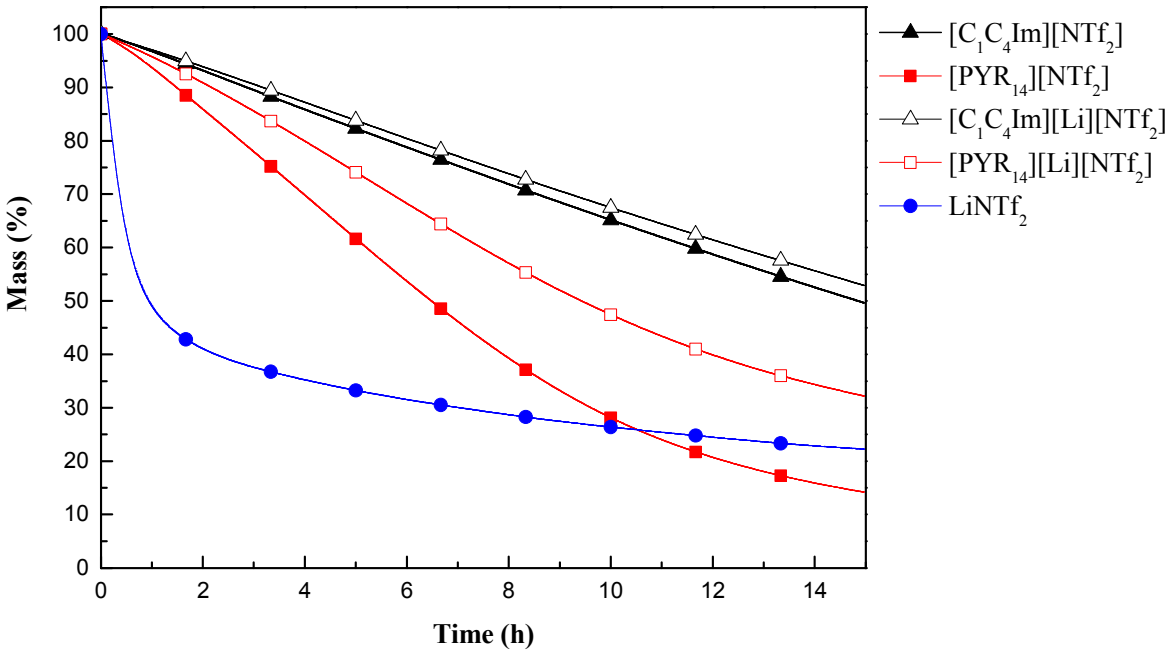
Mass (%)
Time (h)
0
10
20
30
40
50
60
70
80
90
100
0
2
4
6
8
10
12
14
[C1C4Im][NTf2]
[PYR14][NTf2]
[C1C4Im][Li][NTf2]
[PYR14][Li][NTf2]
LiNTf2

Figure 8:

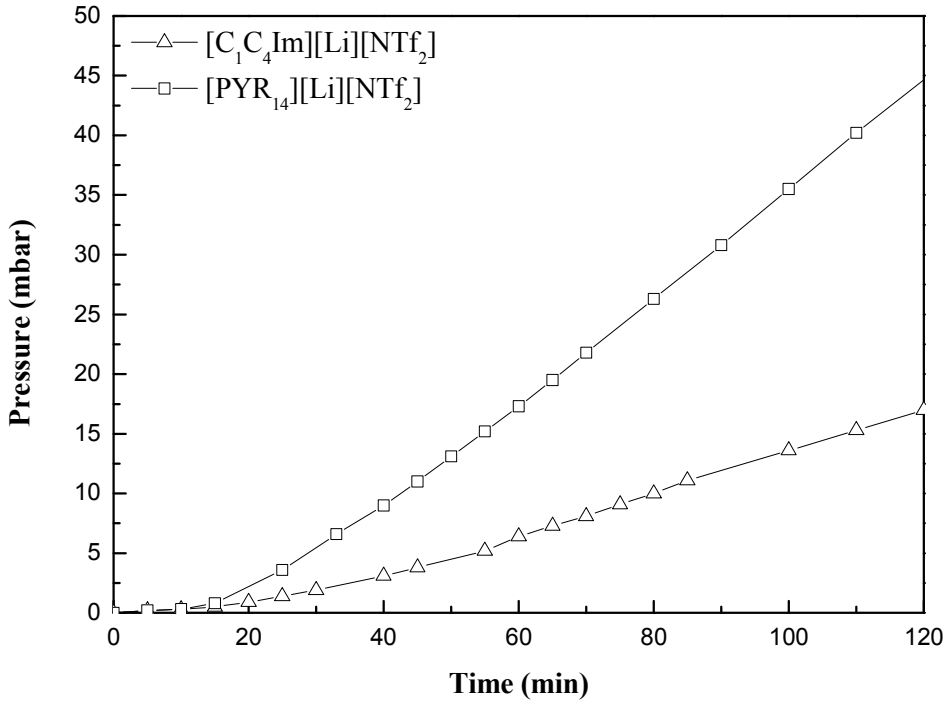
[C1C4Im][Li][NTf2]
[PYR14][Li][NTf2]
Pressure (mbar)
Time (min)
0
5
10
15
20
25
30
35
40
45
50
0
20
40
60
80
100
120

Figure 9:

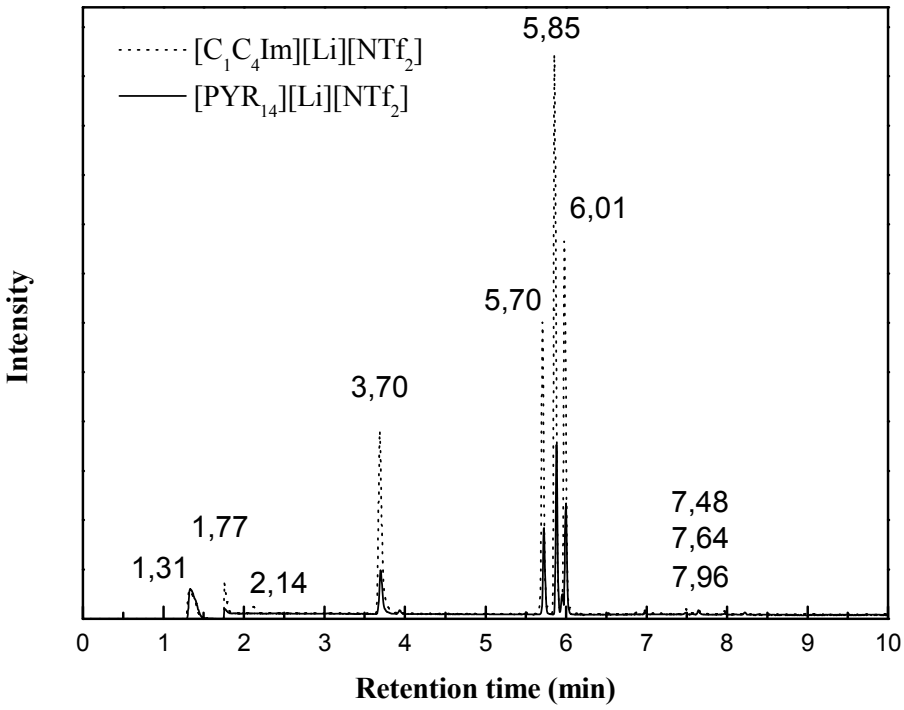
[C1C4Im][Li][NTf2]
[PYR14][Li][NTf2]
5,85
6,01
5,70
3,70
7,48
7,64
7,96
1,77
1,31
2,14
Intensity
Retention time (min)
0
1
2
3
4
5
6
7
8
9
10

Figure 10:

Figure 11:

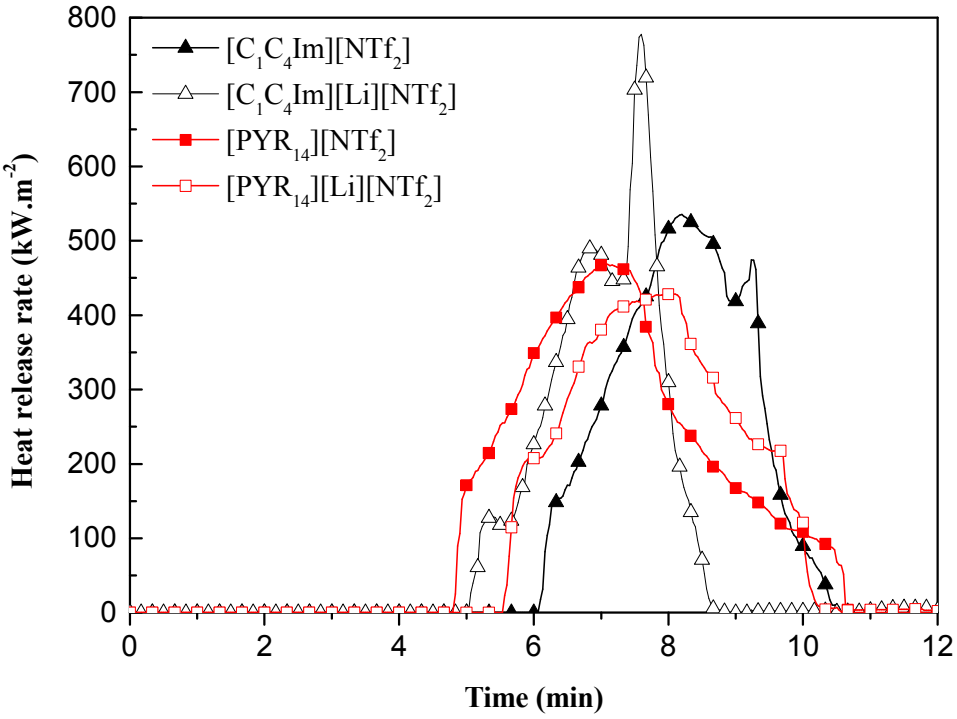
[C1C4Im][NTf2]
[C1C4Im][Li][NTf2]
[PYR14][NTf2]
[PYR14][Li][NTf2]
Heat release rate (kW.m-2)
Time (min)
0
100
200
300
400
500
600
700
800
0
2
4
6
8
10
12

Figure 12:

Table 1: Start and onset temperatures with heats of decomposition of lithium salt, ionic liquids and electrolytes as determined from DSC experiments

Product	$[C_1C_4Im][NTf_2]$	$[PYR_{14}][NTf_2]$	$[C_1C_4Im][Li][NTf_2]$	$[PYR_{14}][Li][NTf_2]$	$LiNTf_2$
T_{onset} (°C)	451	451	456	452	395
T_{start} (°C)	425	403	420	400	355
Heat ($J.g^{-1}$)	1644	1579	1406	1470	854

Table 2: Onset and start temperatures for electrolyte components decomposition as determined from dynamic TGA experiments

Product	$[C_1C_4Im][NTf_2]$	$[PYR_{14}][NTf_2]$	$[C_1C_4Im][Li][NTf_2]$	$[PYR_{14}][Li][NTf_2]$	$LiNTf_2$
T_{onset} (°C)	427	423	434	427	369
T_{start} (°C)	360	277	357	339	298

Table 3: Slopes of mass loss curves in % per h between 2 and 10 h at 350 °C. * slope during 30 first minutes then during 8 last hours

Product	Mass loss rate (%/h)	R^2
$[C_1C_4Im][NTf_2]$	3,54503	0,99984
$[PYR_{14}][NTf_2]$	7,77356	0,99894
$[C_1C_4Im][Li][NTf_2]$	3,33617	0,99994
$[PYR_{14}][Li][NTf_2]$	5,61302	0,99962
$LiNTf_2$	75 then 0.98 *	0.992 then 0.991*

Table 4: Cationic and anionic fragments in the liquid phase identified by MS

Type of decomposition	Imidazolium fragments	Pyrrolidinium fragments
Alkyl chain removal	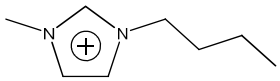 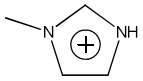 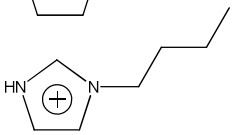	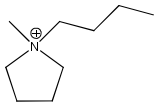  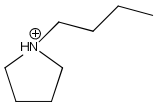
Redistribution	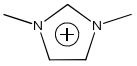 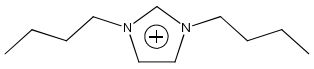	 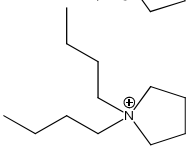
Anion fragments	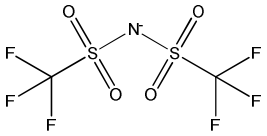 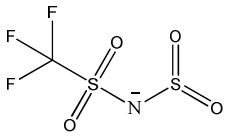	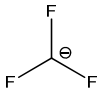 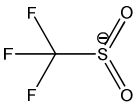

Table 5: Burning behaviour of $[C_1C_4Im][NTf_2]$, $[PYR_{14}][NTf_2]$, $[C_1C_4Im][Li][NTf_2]$ and $[PYR_{14}][Li][NTf_2]$

	$[C_1C_4Im][NTf_2]$	$[PYR_{14}][NTf_2]$	$[C_1C_4Im][Li][NTf_2]$	$[PYR_{14}][Li][NTf_2]$
External flux ($kW.m^{-2}$)	50 then 25	50 then 25	50 then 25	50 then 25
Initial mass (g)	59.3	51.3	61.9	65.1
Mass lost (%)	85.5	94.3	85.1	92.6
Time to ignition (s)	357	280	294	330
Average mass loss rate ($g.m^{-2}.s^{-1}$)	38	24	46.6	36
Heat of combustion ($MJ.kg^{-1}$)				
Lower heating value (LHV)	13.3	14.8	10.78	12.05
Effective heat of combustion (fire calorimetry techniques)	10.0	12.6	7.7	8.2
Energy efficiency (%)	75.2	85.1	71.4	65.6

Table 6: Emission factors of different gases emitted during combustion of neat ILs and corresponding electrolytes

Emission factor ($mg.g^{-1}$)	$[C_1C_4Im][NTf_2]$	$[PYR_{14}][NTf_2]$	$[C_1C_4Im][Li][NTf_2]$	$[PYR_{14}][Li][NTf_2]$
CO_2	746	875	552	531
CO	12.6	29.6	21.6	25.1
Soot	9.7	43.9	11	37.7
THCs	3.3	11.2	4.8	0.6
SO_2	313	310	353	317
NO	6.9	5.1	4.9	3.0
N_2O	1.3	2.2	1.9	1.3
HF	246.1	229.5	294.8	216.6
HCN	2.8	6.7	6.9	8.3

Targeting adequate thermal stability and fire safety in selecting ionic liquid-based electrolytes for energy storage †

L. Chancelier,[a,b] A.O. Diallo,[c,d] C.C. Santini,*[a] G. Marlair,*[c] T. Gutel,[b] S. Mailley,[b] C. Len[d]

(a) UMR 5265 CNRS-Université de Lyon 1-ESCPE Lyon,

43 Boulevard du 11 Novembre 1918, 69616 Villeurbanne, France

(b) LMB, CEA - LITEN, 17 rue des martyrs, 38054 Grenoble, France

(c) Institut National de l'Environnement Industriel et des Risques (INERIS), Parc Technologique Alata, BP2, 60550 Verneuil-en-Halatte, France

(d) UTC–ESCOM, EA 4297, TIMR, Centre de Recherches de Royallieu, BP 20529, 60205 Compiègne, France

† Electronic Supplementary Information (ESI) available

Corresponding author: catherine.santini@univ-lyon1.fr

SI-1: Synthesis of the electrolytes

The 1-butyl-3-methylimidazolium chloride was synthetized following this procedure. N-methylimidazole (99 %wt) was purchased from Sigma Aldrich and purified by distillation. Butylchloride (1.3 equivalent, Sigma Aldrich, 99 %wt) and N-methylimidazole (1 equivalent) were mixed without solvent at 70 °C during 3 days. The resulting IL was a white solid and was washed and recrystallized in toluene at 0 °C. Finally, this $[C_1C_4Im][Cl]$ was dried under primary vacuum at ambient temperature for 24 h. The chemical structure and the purity of the $[C_1C_4Im][Cl]$ were checked by ^1H and ^{13}C NMR. The 1-butyl-1-methylpyrrolidinium chloride (98 %) was purchased from Solvionic and used as received.

The NTf_2-based ILs were prepared by mixing 1 equivalent of the chloride IL with 1.1 equivalent of lithium bis(trifluoromethanesulfonylimide) ($LiNTf_2$) salt (Solvionic, 99.5 %wt, dried at 120 °C under high vacuum for 48 h) in water at ambient temperature for 24 hours. After several extractions with dichloromethane (Aldrich, 99.8 %), the absence of chloride anion was tested using silver nitrate. It was then filtered through silica, and the solvent was evaporated under vacuum. The NTf_2-based ILs $[C_1C_4Im][NTf_2]$ and $[PYR_{14}][NTf_2]$ were vacuum-dried at room temperature for 48 h under 10^{-5} mbars followed by a storage in an argon-filled glove box. The structure was checked by ^1H and ^{13}C liquid NMR

Bruker Avance 300 with probe BBO 5 mm at 27 °C, using deuterated dichloromethane as solvent. Standard 5 mm borosilicate NMR tubes were used. Chemical shifts were reported in ppm (singlet = s, doublet = d, and multiplet = m). Impurity levels of the ILs were then measured. Their water content was lower than 60 ppm (mass ratio), as assessed by Karl Fisher coulometric titration. The chloride content was lower than 0.5 % as shown by mass spectroscopy.

The electrolytes were prepared by adding $LiNTf_2$ (1 $mol.L^{-1}$) in a well stirred and dried IL at room temperature, and will be referred to as $[C_1C_4Im][Li][NTf_2]$ and $[PYR_{14}][Li][NTf_2]$. Finally the neat ILs and electrolytes were vacuum-dried at room temperature for 48 h under 10^{-5} mbars followed by storage in an argon-filled glove box.

SI-2: NMR characterisation of the ILs

$[C_1C_4Im][NTf_2]$

^1H NMR

δ = 0.990 (t, 3H, N-$(CH_2)_3$-C**H**$_3$), 1.395 (m, 1.99H, N-$(CH_2)_2$-C**H**$_2$-CH_3), 1.880 (m, 2.00H, N-CH_2-C**H**$_2$-), 3.949 (s, 2.98H, N-C**H**$_3$), 4.190 (t, 2.03H, N-C**H**$_2$-), 5.356 (s, CD_2Cl_2), 7.339 (s, 1.93H, N-C**H**=C**H**-N), 8.640 (s, 0.97H, N=C**H**-N)

^{13}C NMR

δ=13.321 (N-$(CH_2)_3$-**C**H_3), 19.649 (N-$(CH_2)_2$-**C**H_2-CH_3), 32.220 (N-CH_2-**C**H_2-), 36.601 (N-**C**H_3), 50.301 (N-**C**H_2-), 53.867 (m, CD_2Cl_2), 120.221 (m, N-$(SO_2$**C**$F_3)_2$), 122.760 (**C4**H), 124.101 (**C5**H), 136.079 (N=**C**H-N)

$[PYR_{14}][NTf_2]$

^1H NMR

δ = 1.013 (t, 3H, N-$(CH_2)_3$-C**H**$_3$), 1.4375 (m, 2.01H, N-$(CH_2)_2$-C**H**$_2$-CH_3), 1.770 (m, 2.21H, N-CH_2-C**H**$_2$-), 2.268 (m, 4H, N-CH_2-C**H**$_2$-C**H**$_2$-CH_2-N), 3.036 (s, 3.01H, N-**C**H_3), 3.298 (m, 2.04H, N-C**H**$_2$-), 3.506 (m, 4.05H, N-C**H**$_2$-CH_2-CH_2-C**H**$_2$-N), 5.368 (s, CD_2Cl_2)

^{13}C NMR[1]

δ=13.674 (N-$(CH_2)_3$-**C**H_3), 19.908 (N-$(CH_2)_2$-**C**H_2-CH_3), 21.895 (N-CH_2-**C**H_2-**C**H_2-CH_2-N), 26.037 (N-CH_2-**C**H_2-), 48.877 (N-**C**H_2), 53.871 (m, CD_2Cl_2), 65.053 (N-**C**H_3 and N-**C**H_2-CH_2-CH_2-**C**H_2-N), 120.255 (quadruplet, N-$(SO_2$**C**$F_3)_2$)

SI-3: Setup to analyse the decomposition products formed during thermal treatment of the electrolytes $[C_1C_4Im][Li][NTf_2]$ and $[PYR_{14}][Li][NTf_2]$ during 2 h at 350 °C

In the glove box, 3 mL of the electrolytes $[C_1C_4Im][Li][NTf_2]$ and $[PYR_{14}][Li][NTf_2]$ were introduced in an apparatus depicted below. They were dried under high vacuum (10^{-5} mbar) overnight before the experiment. A blank was collected for the Infrared (IR) spectra of the system using the connected IR cell. The entire system was put under vacuum, with 4 valves open. The reactor was then isolated closing valve 4. The solution was heated by a tubular oven at 10 °C.min^{-1} up to 350 °C. It was kept for 2 hours at this temperature while the pressure of the emitted gas was measured (by the pressure sensor). At the end of the two hours, valve 2 and 3 were closed and the system was cooled down to room temperature.

The system was disconnected from the vacuum line (at valve 4). The gaseous phase was analysed by infrared spectroscopy. Gas aliquots were taken up by closing valve 1 and introducing a syringe by the septum. To reproduce the analysis, the system was purged up to valve 1 (closing valve 1, open 4th and 2nd), gas was brought to the antechamber by closing valve 2 and opening 1 and taken through the septum. The gas samples were analysed by GC and GC-MS. After the gas phase analysis, the schlenk was disconnected from the IR cell in a glove box, and the liquid phase was analysed by ^{1}H, ^{13}C, ^{19}F and ^{7}Li liquid NMR, and by coupled GC-MS.

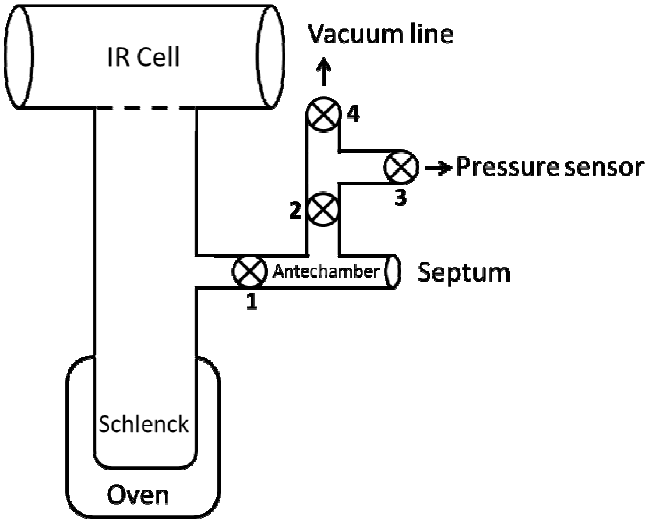

SI-4: GC chromatogram of $[C_1C_4Im][Li][NTf_2]$ (top) and $[PYR_{14}][Li][NTf_2]$ (bottom) on KCl on alumina column

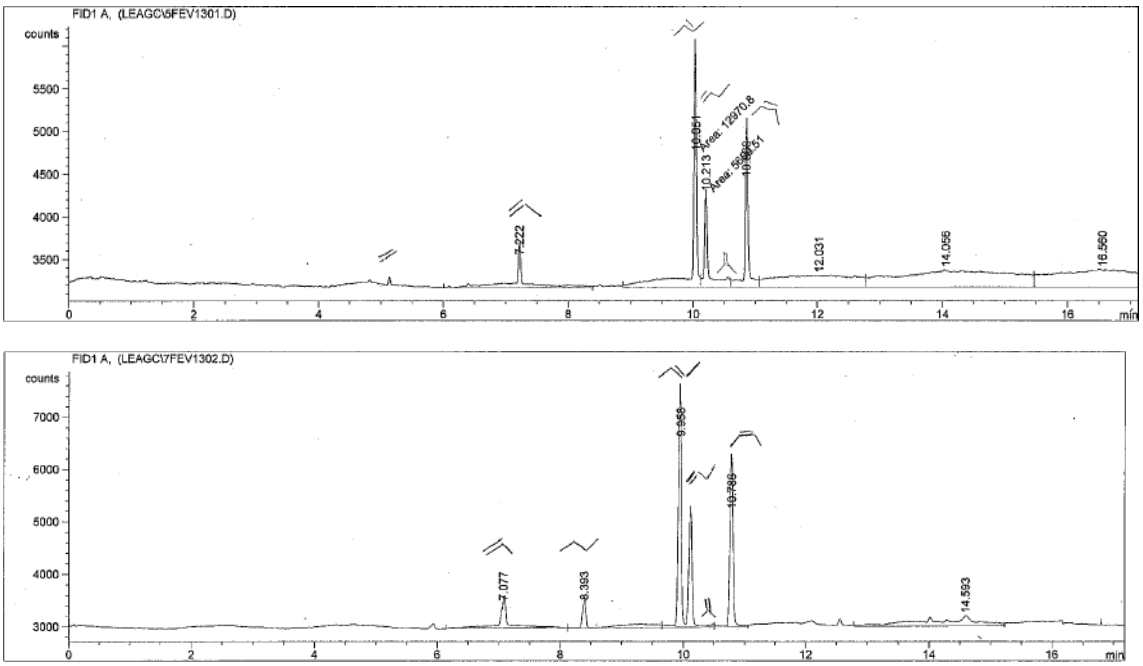

SI-5: Decomposition mechanisms of imidazolium and pyrrolidinium cations [2,3]

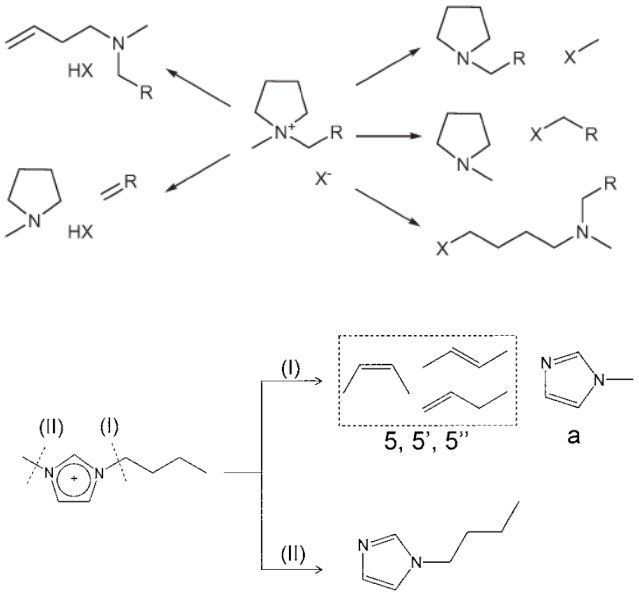

SI-6: Infrared spectra of electrolytes gas phase (after blank subtraction)

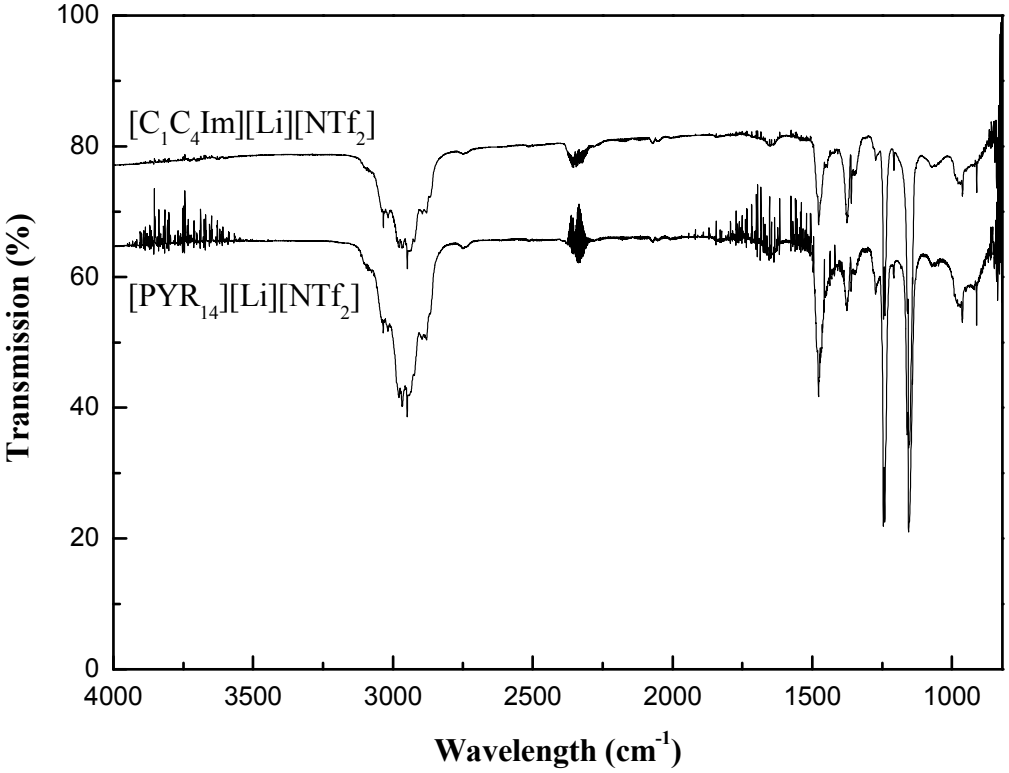

SI-7: Liquid phase study by ^{1}H, ^{13}C, ^{19}F and ^{7}Li solution NMR

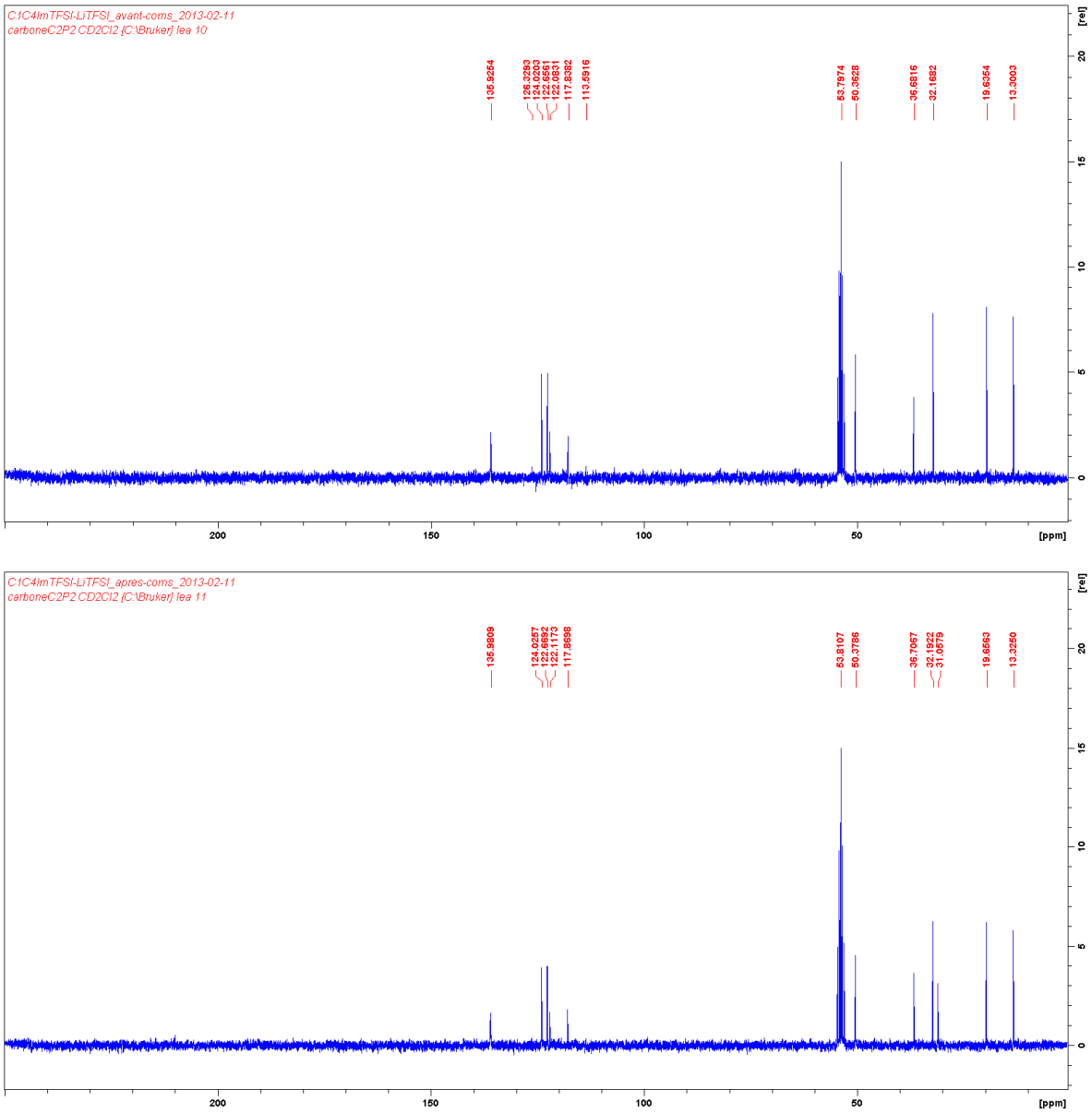

^{13}C NMR spectra of $[C_1C_4Im][Li][NTf_2]$ before (top) and after (bottom) thermal treatment

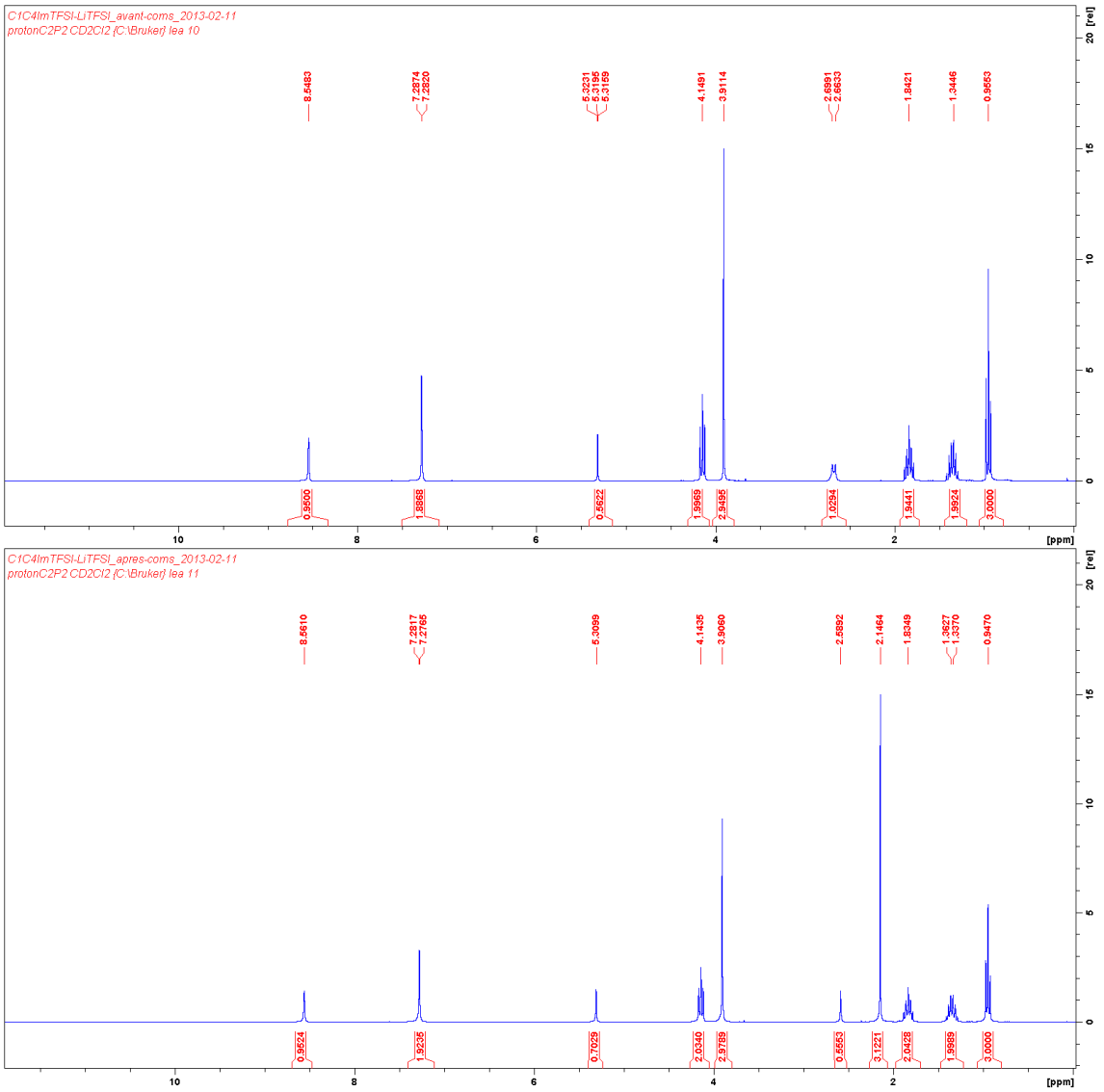

^{1}H NMR spectra of $[C_1C_4Im][Li][NTf_2]$ before (top) and after (bottom) thermal treatment

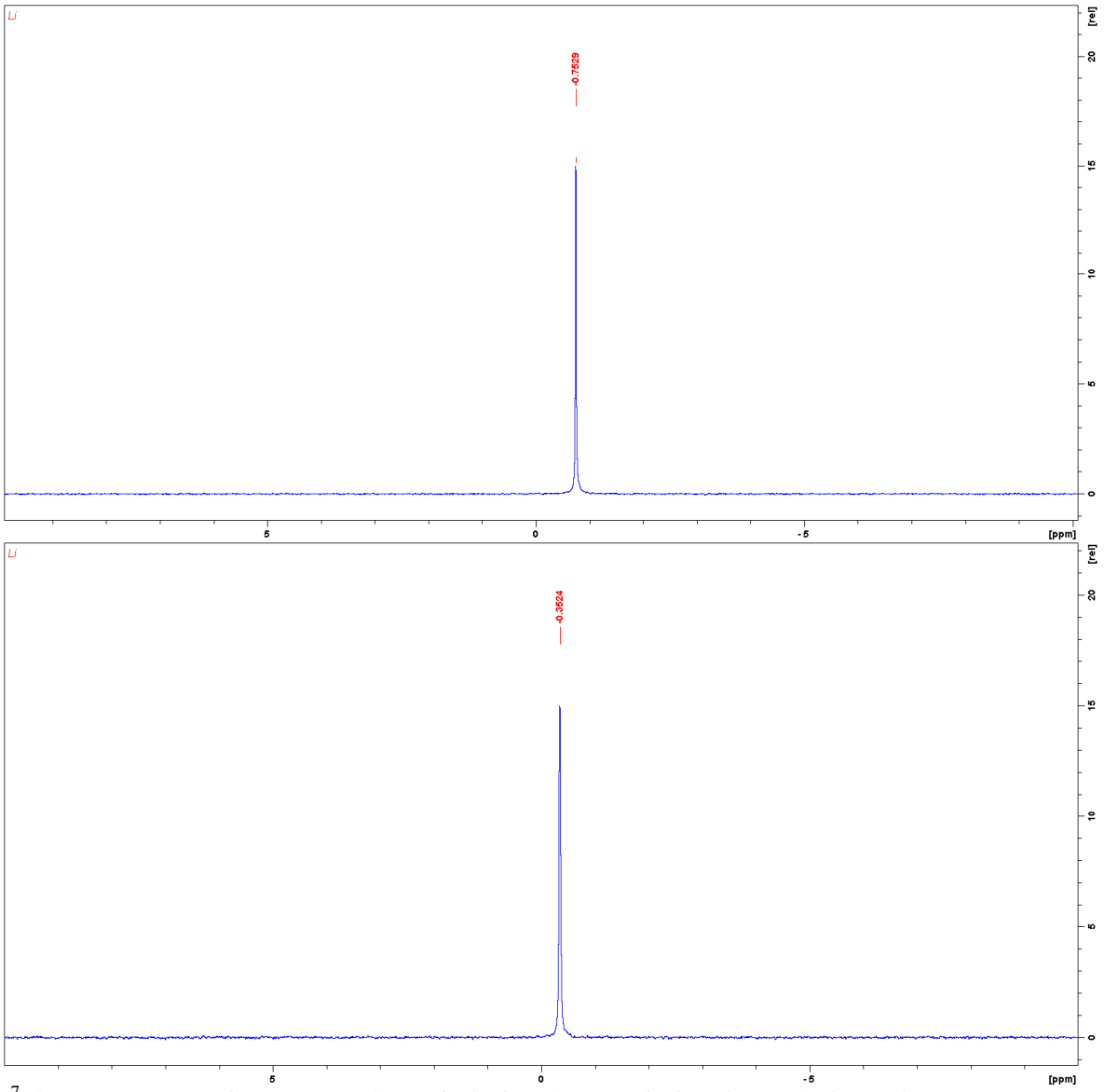

^{7}Li NMR spectra of $[C_1C_4Im][Li][NTf_2]$ before (top) and after (bottom) thermal treatment

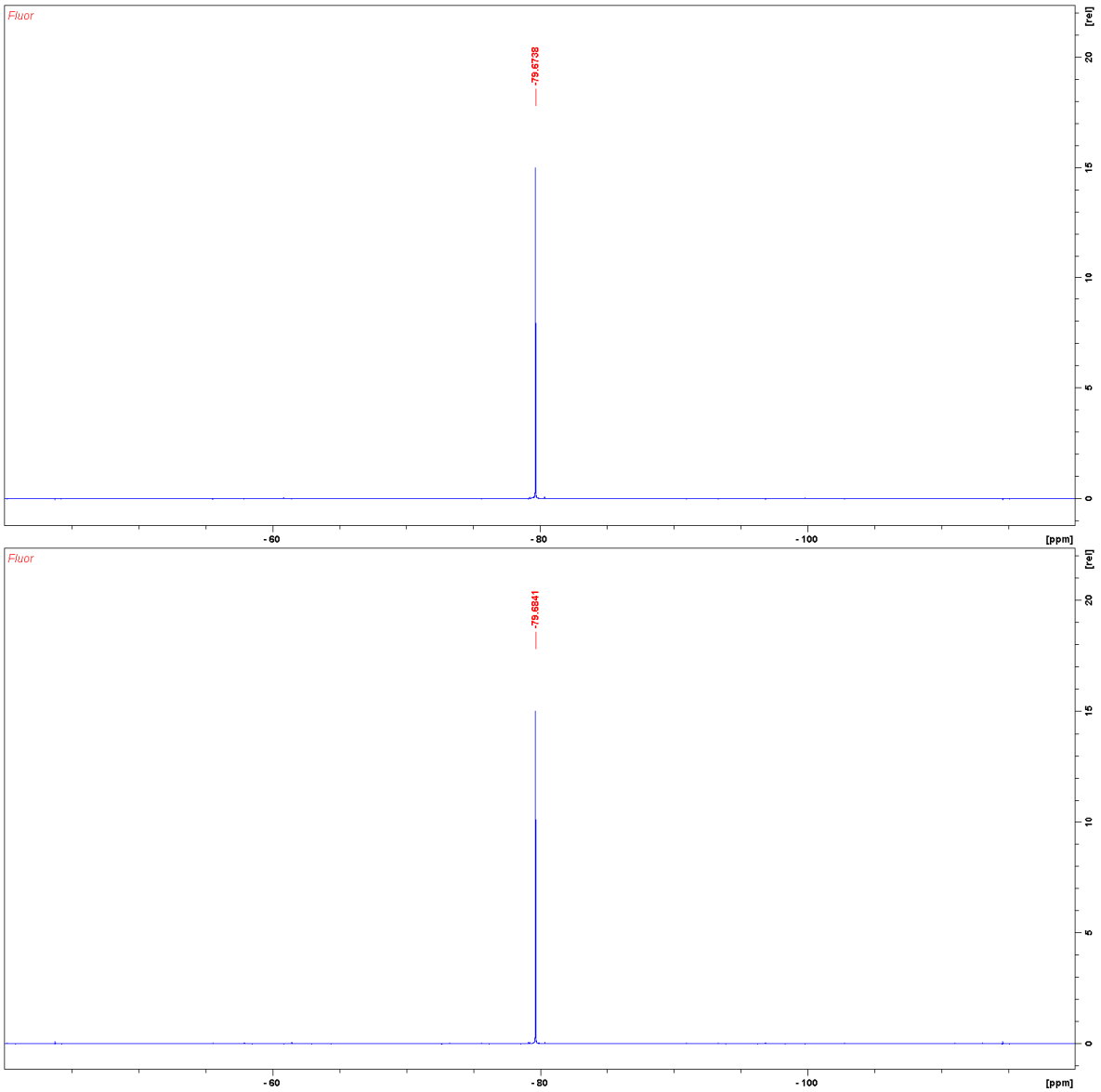

^{19}F NMR spectra of $[C_1C_4Im][Li][NTf_2]$ before (top) and after (bottom) thermal treatment

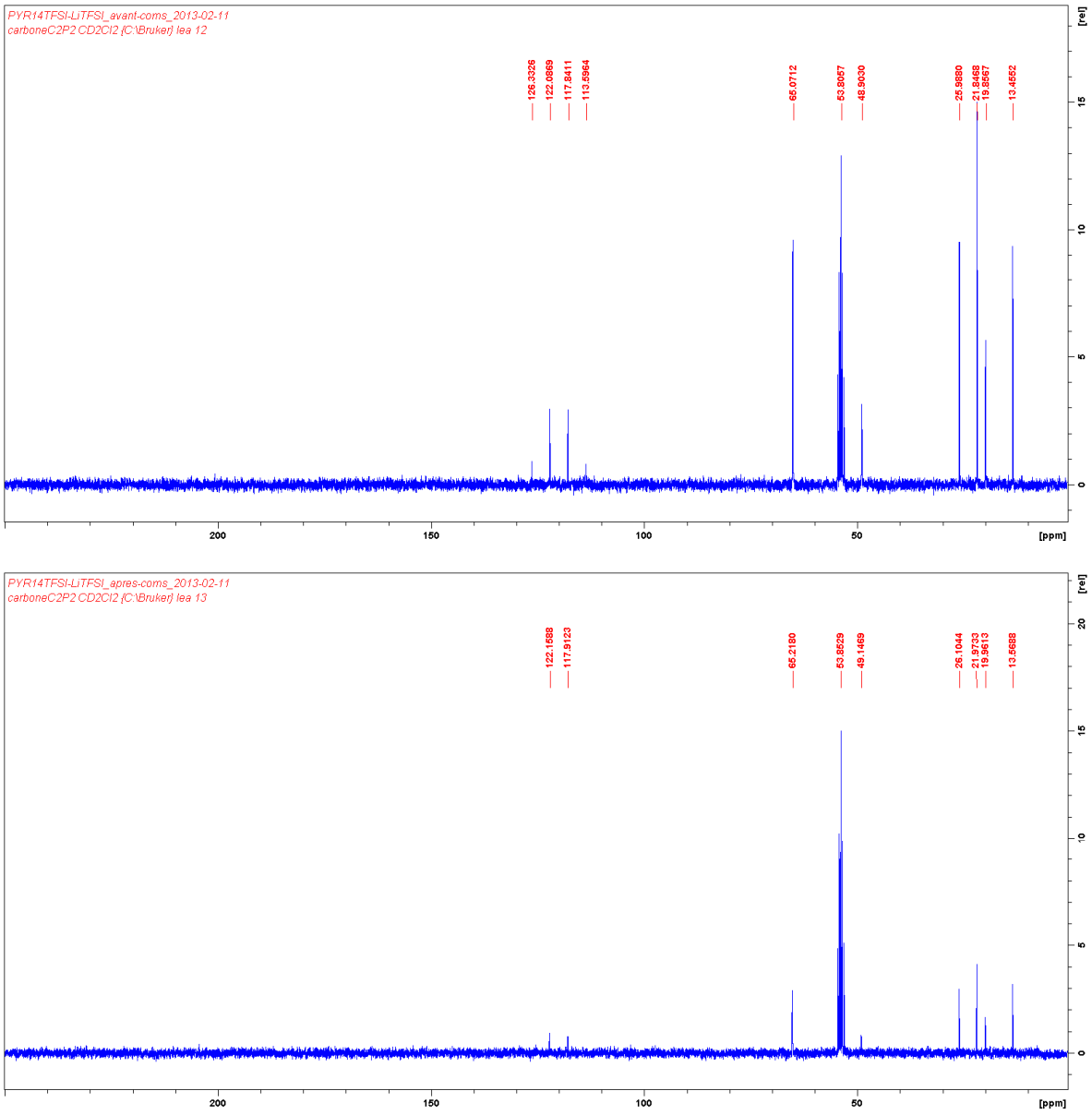

^{13}C NMR spectra of [PYR_{14}][Li][NTf_2] before (top) and after (bottom) thermal treatment

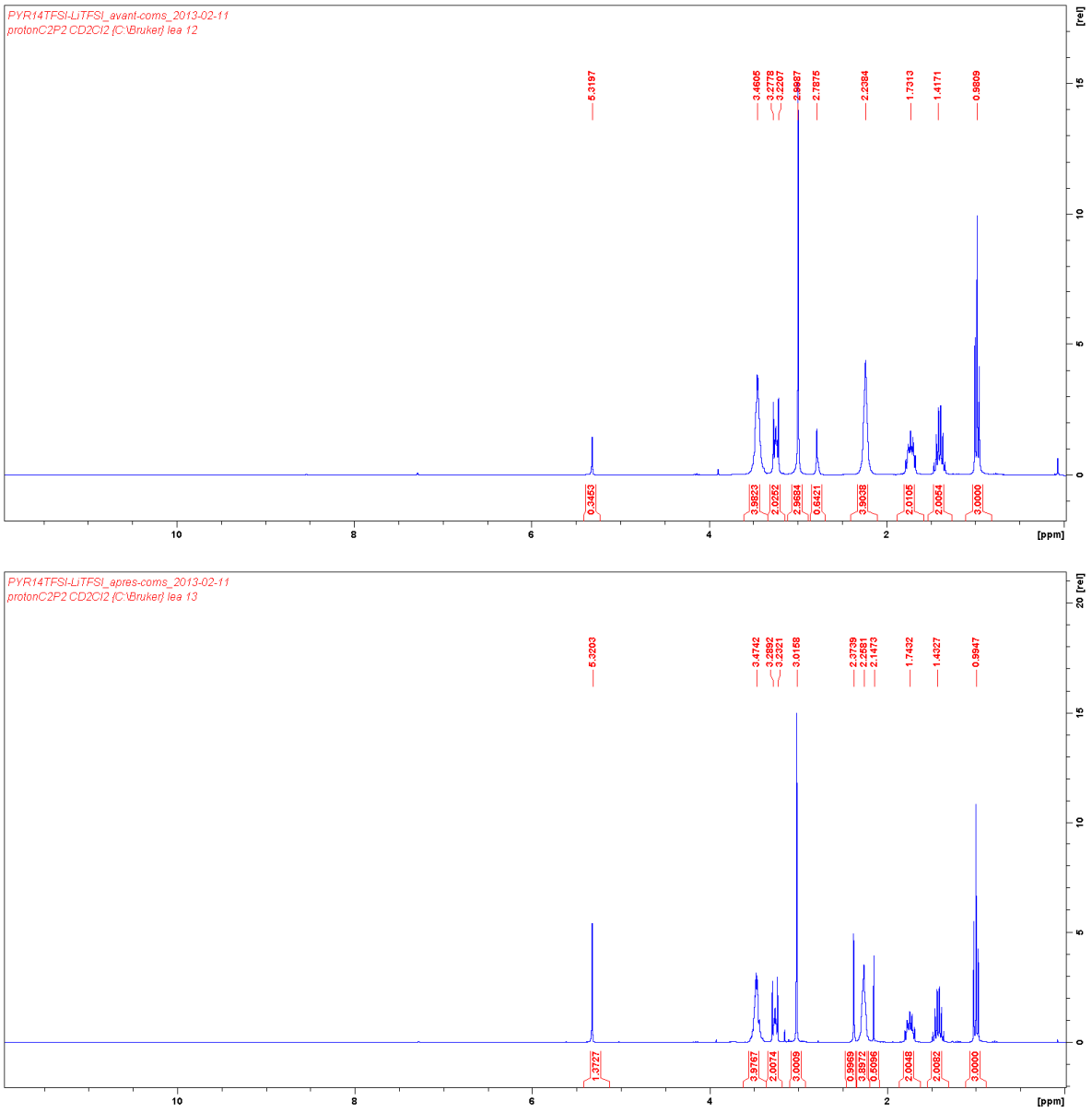

^{1}H NMR spectra of [PYR_{14}][Li][NTf_2] before (top) and after (bottom) thermal treatment

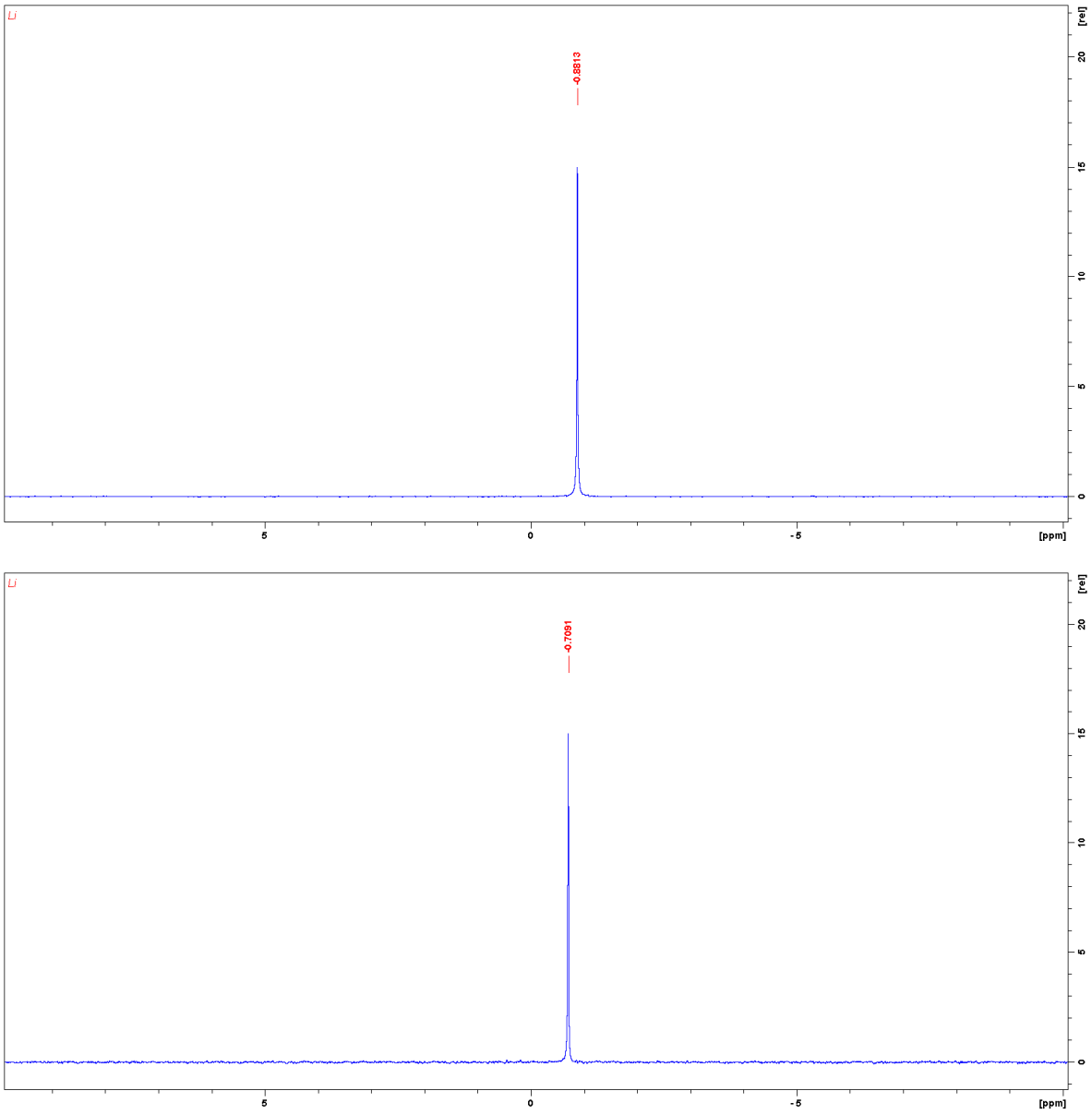

^{7}Li NMR spectra of $[C_1C_4Im][Li][NTf_2]$ before (top) and after (bottom) thermal treatment

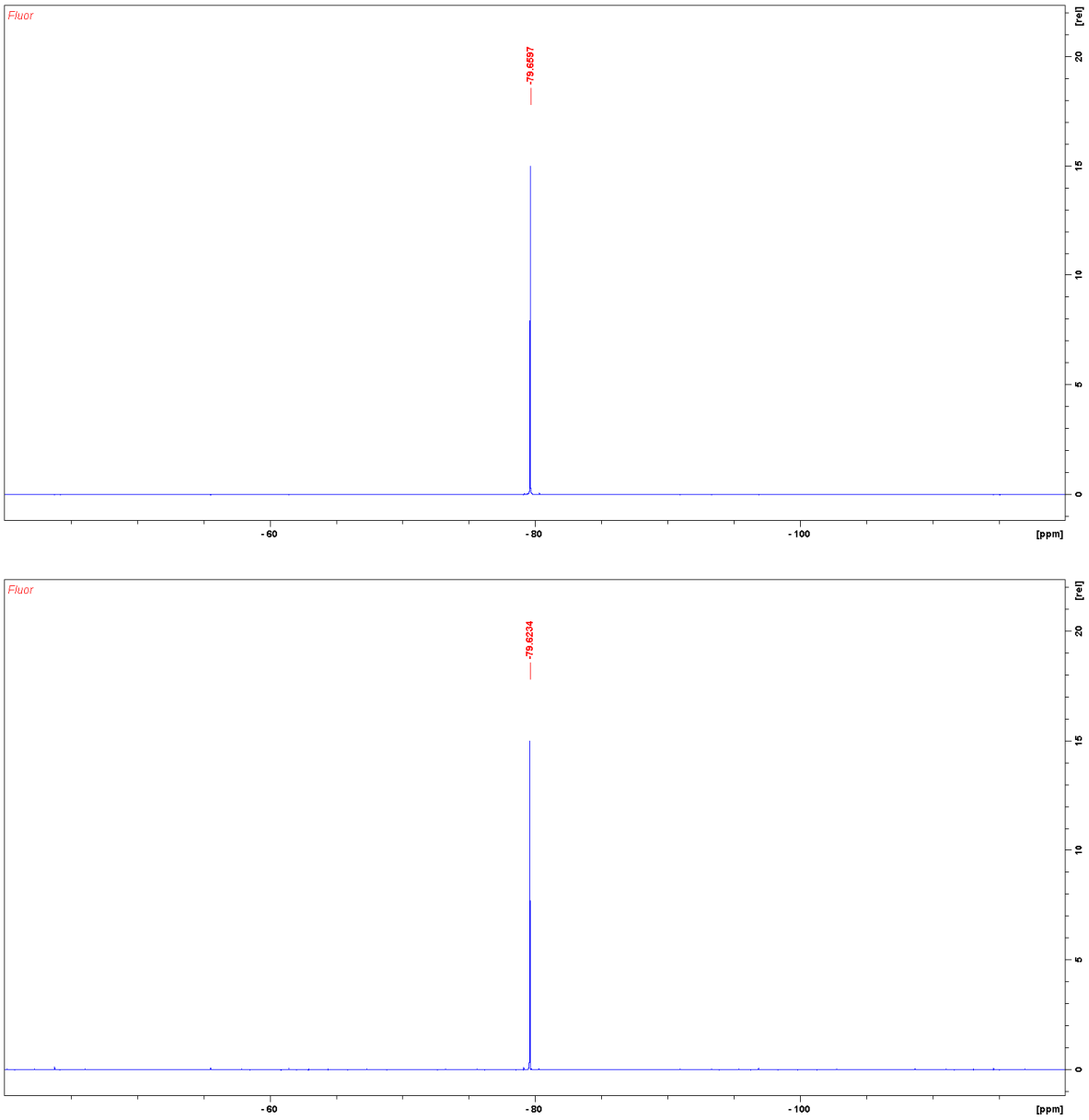

^{19}F NMR spectra of $[C_1C_4Im][Li][NTf_2]$ before (top) and after (bottom) thermal treatment

SI-8 Data validation from the Tewarson tests

It is a routine practice in the lab where the Tewarson apparatus is used to check validity of data from the calculation of mass balance regarding main elements contained in the test samples.

	$[C_1C_4Im][NTf_2]$	$[PYR_{14}][NTf_2]$	$[C_1C_4Im][Li][NTf_2]$	$[PYR_{14}][Li][NTf_2]$
Initial mass (g)	59,3	51,3	61,9	65,1
Residual mass (g)	8,6	2,9	9,2	4,8
	% of element in the residue			
Carbon	49,8	60,9	50,1	55,6
Fluorine	8,7	9,9	11,1	10,1
Sulphur	5,5	7,1	4,4	3,2
	Mass of residue (g)			
Carbon	4,28	1,77	4,61	2,67
Fluorine	0,75	0,29	1,02	0,48
Sulphur	0,47	0,21	0,40	0,15
	Conversion efficiency without residue (%)			
Carbon	66	92,5	59,1	69,3
Fluorine	73,5	76,1	81,3	65,6
Sulphur	86,9	98,2	91,8	89,7
	Conversion efficiency with residue (%)			
Carbon	91,5	103,6	88,6	84,3
Fluorine	78,2	78,2	86,9	68,1
Sulphur	92,1	100,9	95,8	91,1

Carbon and sulphur balance examination

Carbon and sulphur recovery efficiencies from sample content into identified carbonated or S-containing species (in flue gas) or as C or S content (in solid residues) lied in between 84% and 103 % for carbon and 91 % to 101 % for sulphur respectively. This confirmed to our experience (several thousand test runs with the *Tewarson Apparatus*) that no special concern in the performance of the experiments and related data computations appeared. From dedicated analysis of fire calorimetry accuracy analysis, we know that, at lab scale, errors in yields of energy and product releases may be in the order of some 5 to 10%. Accuracy varies according to complexity of test samples (decreasing with complexity of structure and number of hetero-atom in test molecules) and operating conditions. Such error levels keep however quite reasonable for fire safety engineering purposes, owing to complexity of fire phenomena.

Fluorine balance examination

Observed conversion efficiency is thought reasonable, although classically lower than for carbon and sulphur mass balances. Although latest standards for the sampling and measurements are applied routinely (by use of ISO standards developed by ISO TC92 SC3 Committee: *Fire Threat to People and the Environment*), we are confronted here to

potentially non identified species in the flue gas, or absorption issues in apparatus hood and ducting system and/or sampling line.

References

1. J. Golding, S. Forsyth, D. R. MacFarlane, M. Forsyth and G. B. Deacon, *Green Chem.*, 2002, **4**, 223-229.
2. T. J. Wooster, K. M. Johanson, K. J. Fraser, D. R. MacFarlane and J. L. Scott, *Green Chem.*, 2006, **8**, 691-696.
3. H. Ohtani, S. Ishimura and M. Kumai, *Anal. Sci.*, 2008, **24**, 1335-1340.

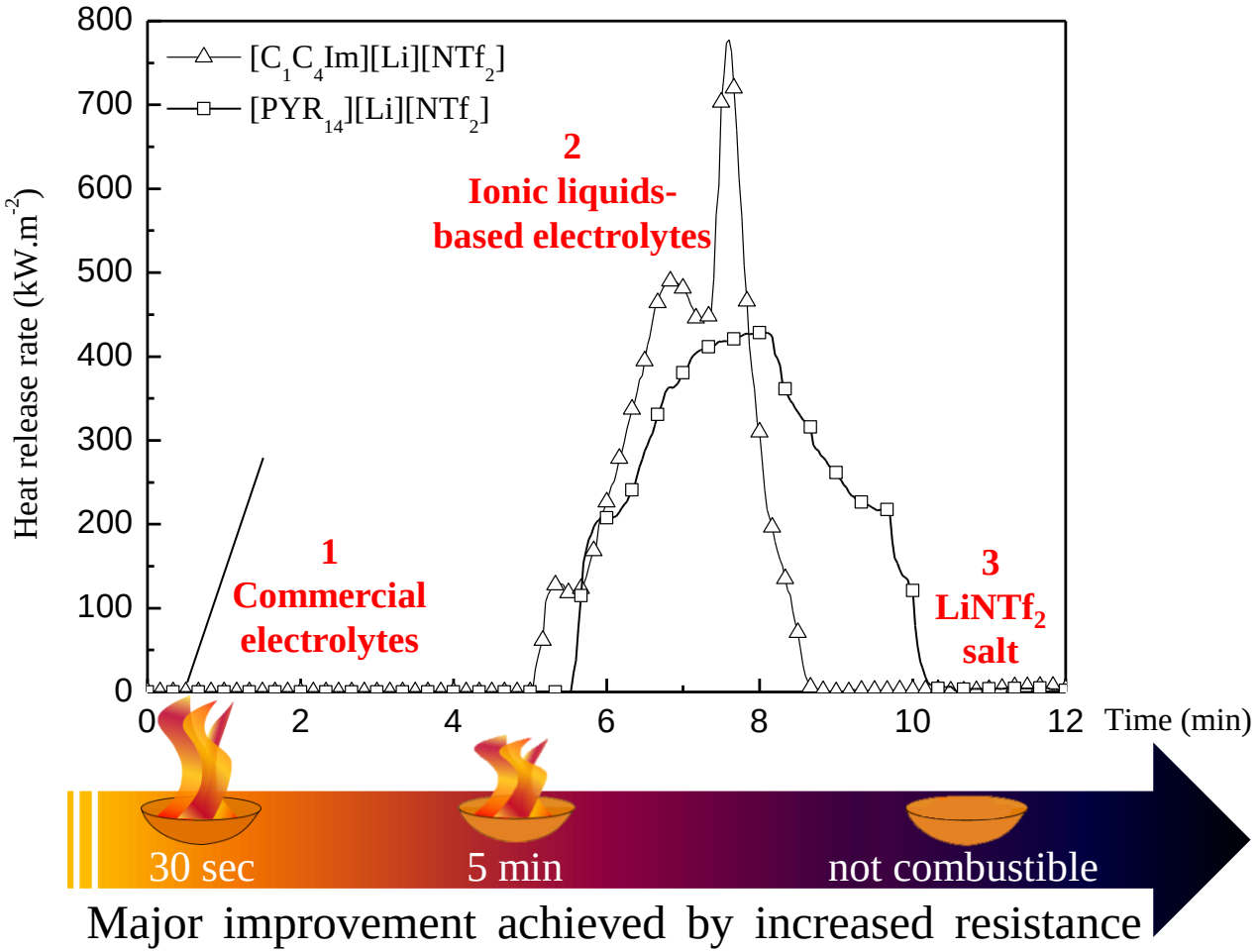

Major improvement achieved by increased resistance to ignition when replacing carbonates by ionic liquids as electrolyte solvents